Journal of Water Process Engineering 75 (2025) 107914

Contents lists available at ScienceDirect

Journal of Water Process Engineering

journal homepage: www.elsevier.com/locate/jwpe

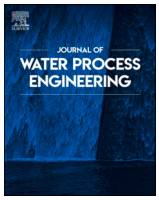

Enhancing single and multi-component adsorption efficiency of pharmaceutical emerging contaminants using bio waste-derived carbon materials and geopolymers

Ana Paula Ferreira [a,b,*], Arthur P. Baldo [a,c], Adriano S. Silva [a,d,e], Ana Paula S. Natal [a,c], Ana J.B. Bezerra [a,c], Jose L. Diaz de Tuesta [f,g], Pricila Marin [c], José A. Peres [b], Helder T. Gomes [a,**]

[a] CIMO, LA SusTEC, Instituto Politécnico de Bragança, Campus de Santa Apolónia, 5300-253 Bragança, Portugal
[b] Chemistry Center of Vila Real (CQVR), University of Trás-os-Montes and Alto Douro, Quinta de Prados, 5000-801 Vila Real, Portugal
[c] Universidade Tecnológica Federal do Paraná (UTFPR), Londrina 86036-370, Brazil
[d] ALiCE – Associate Laboratory in Chemical Engineering, Faculty of Engineering, University of Porto, Rua Dr. Roberto Frias, 4200-465 Porto, Portugal
[e] Research Centre in Digitalization and Intelligent Robotics (CeDRI), Instituto Politécnico de Bragança, Campus de Santa Apolónia, 5300-253 Bragança, Portugal
[f] Chemical and Environmental Engineering Group, ESCET, Universidad Rey Juan Carlos, c/Tulipán s/n, 28933 Móstoles, Spain
[g] Instituto de Investigación de Tecnologías para la Sostenibilidad, Universidad Rey Juan Carlos, C/Tulipán s/n, 28933 Móstoles, Spain

ARTICLE INFO

Editor: Andreina García

Keywords:
CECs
Wastewater treatment
Waste valorization
Environmental remediation
Circular economy
Activated carbon
Carbon nanotubes
Geopolymer

ABSTRACT

Water contamination with pharmaceuticals like acetaminophen (ACT), sulfamethoxazole (SMX), and phenolic compounds such as gallic acid (GA), have become a global concern. These contaminants are persistent environmental pollutants that threaten aquatic life and human health. Adsorption is recognized as an efficient and low-cost solution to tackle water pollution. In this study, the efficiency of three adsorbents—activated carbon (AC), geopolymer (GP), and carbon nanotubes (CNT) prepared from solid wastes for the removal of ACT, SMX, and GA by adsorption is assessed. AC, GP and CNT are synthesized from real wastes to address solid waste management needs. Physisorption confirmed AC superior BET surface area (527 $m^2\ g^{-1}$), followed by CNTs (66 $m^2\ g^{-1}$) and GPs (30 $m^2\ g^{-1}$), allowing to achieve the highest adsorption capacity: 126.8 mg g^{-1} for ACT, 54.9 mg g^{-1} for SMX, and 151.5 mg g^{-1} for GA, with respective breakthrough times of 314, 66, and 68 min. Kinetic and isotherm adsorption models are fitted for all pair pollutant-adsorbent reaching 33 equations to accurately predict adsorption process, concluding that pseudo-second-order kinetic and Freundlich model best fit experimental data, demonstrating a strong adsorbent-adsorbate affinity. The findings suggest that these sustainable materials offer promising solutions for treating contaminated water.

1. Introduction

In the European Union, the growing presence of contaminants of emerging concern (CECs) in natural water bodies has become a critical environmental and public health issue [1,2]. Despite stringent water quality directives, such as the Water Framework Directive (2000/60/EC) [3] and the Urban Wastewater Treatment Directive (91/271/EEC) [4], current wastewater treatment plants (WWTP) are not fully equipped to efficiently remove a wide range of CECs [5,6]. These compounds, including various chemical substances [7], such as antibiotics [8], persistent organic pollutants [9], pharmaceuticals [10], personal care products [11], and endocrine-disrupting chemicals. CECs primarily

Abbreviations: ACT, Acetaminophen; AC, Activated carbon; CNT, Carbon nanotubes; CVD, Chemical vapor deposition; CECs, Contaminants of emerging concern; DTG, Derivative thermogravimetric analysis; EOP, Exhausted olive pomace; FA, Fly ash; FT-IR, Fourier transform infrared spectroscopy; GA, Gallic acid; GPs, Geopolymers; HPLC, High-performance liquid chromatography; ICP-OES, Inductively coupled plasma optical emission spectroscopy; LDPE, Low-density polyethylene; pH_{PZC}, Point of zero charge; SMX, Sulfamethoxazole; TCD, Thermal conductivity detector; TGA, Thermogravimetric analysis; WWTP, Wastewater treatment plants; XRD, X-ray diffraction.

* Correspondence to: CIMO, LA SusTEC, Instituto Politécnico de Bragança, Campus de Santa Apolónia, 5300-253 Bragança, Portugal.
** Corresponding author.
E-mail addresses: anapaula.silva@ipb.pt (A.P. Ferreira), htgomes@ipb.pt (H.T. Gomes).

https://doi.org/10.1016/j.jwpe.2025.107914
Received 26 February 2025; Received in revised form 3 May 2025; Accepted 7 May 2025
Available online 15 May 2025

originate from anthropogenic activities [12], and their extensive occurrence [13], persistence [14], bioaccumulation [5], and continuous circulation and transformation within aquatic ecosystems [15] have raised substantial global concern [16].

Among pharmaceutical compounds classified as CECs, paracetamol (ACT) (acetaminophen, 4-acetaminophen-nol) [17] due to its widespread use as an over-the-counter analgesic and antipyretic [18], leading to its frequent detection in wastewater effluents and natural water bodies [19]. Another example of CECs belonging to the pharmaceutical group is sulfamethoxazole (SMX) [1] an antibiotic commonly used to treat bacterial infections in the respiratory, gastrointestinal, and genitourinary tracts [20]. SMX has been frequently detected in various aquatic environments [21] due to its widespread use in human and veterinary medicine [20]. SMX and ACT are persistent and resistant to conventional wastewater treatment processes [22]. Its presence in the environment poses risks to aquatic organisms, contributing to antibiotic resistance development [23], a growing global concern. The compound can also undergo partial transformation in the environment, leading to the formation of metabolites that may be more toxic than the parent compound [24].

In addition to the mentioned contaminants, phenolic compounds (such as gallic acid – GA) are present in several effluents, including industrial [25] (*e.g.,* oil pesticides and herbicides production, pharmaceuticals, plastics, and textiles), agricultural [26] and urban wastewater [27]. These compounds can present adverse effects on the water ecosystem even at low concentrations due to their ecotoxicity [28], and treatment solutions are required to ensure that all phenolic-containing effluents are adequately treated before discharge in water bodies.

Creating a new approach to environmental protection across different domains involves using strategies to minimize contaminants in WWTP, such as optimizing biological processes [29], incorporating advanced oxidation techniques [30], electrocoagulation-assisted adsorption [31] and integrating innovative materials [32] for enhanced pollutant removal by optimized adsorption. In this context, adsorption stands out for its efficiency and simplicity. However, only a limited range of adsorbents, such as biochar [33], zeolites [34], and metal-organic frameworks [35], have been investigated for the removal of SMX, PCM, and AG.

One promising strategy is to develop and apply adsorptive materials like activated carbon (AC) [36], geopolymers (GP) [37,38], and carbon nanotubes (CNT) [39], which combined can effectively capture and remove contaminants such as pharmaceuticals [40], heavy metals [37,41], and organic compounds [42] from wastewater streams. ACs, GPs, and CNTs can be derived from real solid waste (RSW), supporting the circular economy by turning residual materials into valuable products [43,44]. ACs, with high porosity, are ideal for adsorption and can be made from agricultural waste (such as exhausted olive pomace - EOP) through slow pyrolysis, offering a sustainable alternative to coal [44]. GPs are eco-friendly, synthesized from industrial by-products like fly ash (FA) [45]. CNTs can be produced from plastic solid waste *via* chemical vapor deposition (CVD), promoting resource recovery and addressing plastic pollution and carbon emissions [44].

Numerous studies focus on batch mode and single adsorbent systems to remove contaminants in tertiary treatment processes at WWTPs, primarily targeting organic compounds, dyes [37], and common pollutants like nitrates [46] and phosphates [47]. However, there is growing demand for research that combines materials with complementary properties, such as AC [48], GPs [49], and CNTs [50], to improve the efficiency and versatility of contaminant removal processes in wastewater treatment.

This work delves into the comparison and adsorptive potential of novel RSW-derived adsorbents (AC, GP, and CNT prepared from exhausted olive pomace, fly ashes and plastic wastes, respectively) in the removal of CECs and phenolic pollutants from wastewater, given technic solution to the challenge of both solid waste and wastewater management. The methodology includes the characterization of the materials to draw connections between the synthesis processes, their physicochemical properties, and their adsorption performance. Furthermore, a comprehensive kinetic and isotherm adsorption modeling, employing pseudo-first, pseudo-second-order, intraparticle diffusion, Freundlich and Langmuir models, is performed to unlock a deeper understanding of the interactions between adsorbents and adsorbates. Upon select the better RSW-derived adsorbents, their synergy is explored in analyses of breakthrough curves for both multi- and single-component pollutants, shedding light on the dynamic behavior of these innovative adsorbents in wastewater treatment.

2. Methodology

2.1. Reagents and materials

The reactants employed in this investigation are shown below and classified according to their specific applications. The simulated wastewater contaminants include ACT ($C_8H_9NO_2$–98 %), provided by Alfa Aesar; SMX ($C_{10}H_{11}N_3O_3S$ – 98 %), provided by Supelco®; and GA ($C_6H_2(OH)_3COOH$ - 98 %), provided by EMD Millipore Corporation. For ACs production, EOP (composition in Table S.1) was provided by Mirabaga; carbon dioxide (CO_2–99 %), supplied by AirLiquide; nitrogen (N_2–99%), provided by AlphagazTM; and silica wool, provided by Elemental Microanalysis. For CNTs production (composition in Table S1), the reagents used included low-density polyethylene (LDPE); nitrogen (N_2–99%), provided by AlphagazTM; aluminum oxide (Al_2O_3–99 %), provided by BASF; ethanol absolute (C_2H_5OH - 99 %), supplied by Fisher Chemical; ethylene glycol ($C_2H_6O_2$–99 %), also provided by Fisher Chemical; iron (II) chloride tetrahydrate ($FeCl_2{\cdot}4H_2O$ – 99 %), provided by Acros Organics; and iron (III) chloride hexahydrate ($FeCl_3{\cdot}6H_2O$ – 97 %), provided by VWR Chemicals. Finally, for GPs production, FA (composition in Table S2) was used, supplied by SOGAMA; sodium hydroxide pearls (NaOH - 98 %), provided by Labkem; sodium silicate (Na_2SiO_3 - Na_2O = 10.6 % and SiO_2 = 26.5 %), provided by Fisher Chemical; and hydrochloric acid (HCl - 37 %), supplied by VWR Chemicals, was used to wash and neutralize the pH of the GPs.

2.2. Materials synthesis method

10 g of EOP (ground and sieved to a particle size smaller than 250 μm) were placed in a tubular furnace with a nitrogen flow of 100 mL min^{-1} to produce AC. A heating ramp of 5 °C min^{-1} was applied, progressing through three temperature stages: 400 °C and 600 °C for 1 h each, followed by 800 °C for 4 h. At 800 °C, the nitrogen flow was replaced with CO_2 injection for 1 h to activate the carbon, following a procedure adapted from elsewhere [51], which provided an optimal balance between surface area development and carbon yield for EOP. Nitrogen was then reintroduced and continued until the reactor cooled. The materials were washed with distilled water until achieving a neutral pH, dried in oven at 40 °C, sieved to obtain a particle size lower than 53 μm, and stored for further use.

CNTs were synthesized *via* the CVD technique, using ferromagnetic nanoparticles supported on alumina. The nanoparticles were initially prepared using a sol-gel method. The process involved the preparation of two solutions: 20 mL of ethanol with 10 mmol of $FeCl_2{\cdot}4H_2O$ and 80 mL of ethylene glycol with 20 mmol of $FeCl_3{\cdot}6H_2O$. These were stirred and heated to 80 and 60 °C, respectively, before being cooled to room temperature. Both solutions were then combined with 6.6 g of alumina, stirred, and gradually heated to 60 °C for 2 h, then to 120 °C until a gel-like consistency was formed, and finally to 210 °C to yield a dry powder. The resulting powder underwent calcination at 300 °C for 12 h, followed by 600 °C for 24 h in an oxidative atmosphere, yielding the iron oxide supported on alumina catalyst (IO). The one-chamber reactor used in the CVD process has three heating zones that can be controlled independently. For the synthesis, the upper crucible (polymer cracking zone)

was loaded with 5 g of the model polymer (LDPE), and the lower crucible (CVD zone) was loaded with 1 g of the IO catalyst. The synthesis procedure was conducted at 850 °C for 1 h with a nitrogen flow of 50 mL min^{-1} [52]. After synthesis, the final CNT material was recovered from the reactor and subjected to acid washing (50 % *v*/v H_2SO_4, 140 °C, 3 h under reflux) to remove residual metal catalysts. The material was then dried and sieved to isolate particles smaller than 53 μm.

GP was prepared using 10 g of FA as the aluminosilicate source. An alkali-activating solution was prepared by mixing 5.67 g of sodium silicate (Na_2SiO_3) and 2.27 g of sodium hydroxide (NaOH). The mixture was cured for 24 h at room temperature. The GPs were then ground into a fine powder for adsorption studies. After grinding, the crushed GP was thoroughly washed multiple times using distilled water and a 0.1 M hydrochloric acid solution until the pH of the solution containing the GP was neutral. Following washing, the GP was dried overnight at 40 °C. The dried GP was then sieved to isolate particles with sizes smaller than 53 μm [53].

2.3. Materials characterization

The chemical composition of FA was determined by inductively coupled plasma optical emission spectroscopy (ICP-OES) analysis using a Vista AX Pro-720ES equipment (Varian, Ontario, Canada). The chemical composition of EOP, AC and CNT was assessed by elemental analysis (CHNS), carried out in a Flash 2000 analyzer (Thermo Fisher Scientific, Massachusetts, USA) equipped with a thermal conductivity detector (TCD).

The textural properties were gathered upon analysis of N_2 adsorption-desorption isotherms at 77 K, obtained in a Quantachrome NOVATOUCH LX4 adsorption analyzer equipped with long cells with a bulb and outer diameter of 9 mm. Before the analysis, the samples were degasified for 16 h at 120 °C, following IUPAC recommendation. Total pore volume (V_T), BET specific surface area (S_{BET}), and Langmuir-specific surface area ($S_{langmuir}$) were gathered using the Quantachrome TouchWinTM software. The external surface area (S_{ext}) and the micropore volume (V_{mic}) were obtained by the t-method (thickness was calculated by employing the ASTM standard D-6556-01). The microporous surface area (S_{mic}) was determined as the subtraction of Sext from S_{BET} and the average pore width (W_{mic}) by approximation ($W_{mic} = 4\ V_{mic}\ S_{mic}^{-1}$). The total pore volume (V_{Total}) was determined at $p/p^0 = 0.98$. Calculations of those methods were all done using the TouchWinTM software v1.21.

The analysis of surface chemistry for the materials was tracked using Fourier Transform Infrared Spectroscopy (FT-IR), with a PerkinElmer FT-IR spectrophotometer UATR Two. The spectra were recorded from 450 to 4000 cm^{-1} with a resolution of 4 cm^{-1}. X-ray diffraction (XRD) measurements were conducted at room temperature using a PANalytical X'Pert Pro diffractometer equipped with an X'Celerator detector and a secondary monochromator in θ/2θ Bragg-Brentano geometry. To assess the material's acid-base properties, various solutions were prepared and titrated to determine acidic and basic sites. To assess the material's acid-base properties, various solutions were prepared and titrated to determine acidic and basic sites. For acidic sites, the samples (0.2 g) were mixed with NaOH (0.02 mol L^{-1}) and then titrated with HCl (0.01 mol L^{-1}). For basic sites, the samples were mixed with HCl (0.02 mol L^{-1}) and then titrated with NaOH (0.01 mol L^{-1}). Acidic site concentration was determined by the moles of NaOH consumed, while basic site concentration was determined by the moles of HCl consumed, both normalized to the sample mass. The following eq. (1 and 2) was used for sites calculations:

$$C_{acidic} = \frac{C_{NaOH} \cdot V_{NaOH} - C_{HCl} \cdot V_{HCl}}{m_{sample}} \quad (1)$$

$$C_{basic} = \frac{C_{HCl} \cdot V_{HCl} - C_{NaOH} \cdot V_{NaOH}}{m_{sample}} \quad (2)$$

where C_{acidic} and C_{basic} (mmol g^{-1}) represents the concentration of acidic or basic sites on geopolymer's surface, C_{NaOH} and C_{HCl} (mmol L^{-1}) are the initial concentrations of NaOH and HCl, respectively, V_{NaOH} (L) is the volume of NaOH added during titration, V_{HCl} (L) is the volume of HCl added during titration, and m_{sample} (g) is the mass of the solid sample used.

To determine the point of zero charge (pH_{PZC}), nine dilutions of NaCl (0.01 mol L^{-1}) were prepared, and their pH was adjusted between 4 and 12 by adding NaOH (0.02 mol L^{-1}) or HCl (0.02 mol L^{-1}). To study pH effects on the material's adsorption performance, 0.15 g of the solid sample was added to each solution and stirred at 300 rpm and 25 °C for 1440 min. After filtration, the pH of the solutions was measured, and the final and initial pH values were plotted to determine the pH at which the surface charge of the adsorbent is zero [54]. Finally, thermogravimetric analysis (TGA) (TGA-DCS1, Mettler-Toledo, SAE) was performed in air atmosphere from 40 to 900 °C (heating rate 10 °C min^{-1}) to evaluate the mass loss for the samples during the synthesis procedure.

2.4. Adsorption tests

2.4.1. Kinetic modeling

The adsorbents were individually loaded (C_{ads} = 2.5 g L^{-1}) into separate pollutants solutions with an initial concentration of C_0 = 100 mg L^{-1}. The pH values of the solutions were measured prior to the experiment, 4.5 for SMX, 3.4 for GA, and 5.6 for ACT. The solution underwent agitation on a magnetic stirrer at 300 rpm. At 13 distinct time intervals (0, 2, 5, 10, 15, 20, 30, 45, 60, 90, 120, 240, and 360 min), 2 mL aliquots were drawn from the solution. This study employed three kinetic models: the pseudo-first-order model, the pseudo-second order, and the intraparticle diffusion model. The mathematical expressions are given, respectively, by Eqs. (3), (4), and (5) [55].

$$q_t = q_e\left(1 - e^{-k_1 t}\right) \quad (3)$$

$$q_t = \frac{q_e^2 k_2 t}{1 + q_e k_2 t} \quad (4)$$

$$q_t = k_{id} t^{1/2} + I \quad (5)$$

where q_t is the adsorption capacity (mg g^{-1}) at a time t (min), q_e is the adsorption capacity at equilibrium (mg g^{-1}), k_1 is the adsorption rate kinetic constant of the pseudo-first-order model (min^{-1}), k_2 is the adsorption rate kinetic constant of the pseudo-second-order model (g mg^{-1} min^{-1}), k_{id} is the intraparticle diffusion rate constant (mg g^{-1} $min^{-0.5}$), and I is the intercept (mg g^{-1}).

2.4.2. Equilibrium isotherms models

The selected adsorbents (C_{ads} = 2.5 g L^{-1}) was tested with eight different concentrations for each pollutant (15, 25, 50, 75, 100, 150, 200, and 400 mg L^{-1}). The mixture was agitated on a magnetic stirrer at 300 rpm at room temperature for 24 h, after which a 2 mL aliquot was collected, filtered with a 0.45 μm Polytetrafluoroethylene syringe filter, and stored for High Performance Liquid Chromatography (HPLC) analysis. Two isotherm fitting models for solid-liquid systems were evaluated: Langmuir and Freundlich [30]. Eq. (6) gives the expression representing the Langmuir model.

$$q_{eq} = \frac{q_{max} K_L C_{eq}}{1 + K_L C_{eq}} \quad (6)$$

where q_{eq} is the adsorption capacity at equilibrium (mg g^{-1}), q_{max} is the maximum adsorption capacity of the adsorbent (mg g^{-1}), C_{eq} is the equilibrium concentration (mg L^{-1}), and K_L is the Langmuir adsorption constant (L mg^{-1}).

In contrast, the Freundlich isotherm model is interpreted as a model for sorption onto a heterogeneous surface that contains sites with

varying affinities [32]. Eq. (7) shows how this model is represented.

$$q_{eq} = K_F C_{eq}^{1/n_F} \tag{7}$$

K_F is the Freundlich constant (L g^{-1}), and n_F is the dimensionless Freundlich constant related to adsorption intensity, values in the range 1 to 10 represent favorable adsorption conditions.

2.4.3. Breakthrough curves and dynamic modeling

These operations were conducted under non-steady-state conditions, with adsorbate concentrations in both the fluid and solid phases varying over time and position within the bed. The steps involved adding in a Labbox 150 mm adsorption column, 20 g of GP, 0.5 g of AC powder, and glass beads, followed by circulating the contaminated solution containing SMX, ACT, and GA (C_0 = 100 mg L^{-1}), (either mixed or separated) using an HPLC pump at a flow rate (Q) of 0.1 mL min^{-1}.

A breakthrough curve is a graphical representation of the concentration of a contaminant in the effluent over time during a fixed-bed adsorption process [56]. It is obtained by plotting the effluent concentration of the adsorbate against the volume of liquid passed through the adsorption column. The time equivalent to the usable capacity of the bed (t_u) and the time equivalent to the total stoichiometric capacity of the packed-bed tower (t_t) if the entire bed reaches equilibrium are provided by a mass balance in the column. The parameter can be calculated using Eq. (8) and Eq. (9):

$$t_u = \int_0^{t_b} \left(1 - \frac{C_A}{C_{A0}}\right) dt \tag{8}$$

$$t_t = \int_0^{t_s} \left(1 - \frac{C_A}{C_{A0}}\right) dt \tag{9}$$

where t_b is the breakpoint, defined as the time when C/C_0 exceeds the limit established, as is the time corresponding to the saturation of the bed, C_A is the concentration in the liquid phase at a given time, and C_{A0} is the initial concentration. If total operation time (t_t) is assumed to be the time equivalent to the usable capacity of the bed (t_u) up to t_b, this ratio is the fraction of the total bed capacity or length utilized to the breakpoint [57]. Hence, the length of the unused bed (H_{UNB}) is the unused fraction times the total length (H_t), given by the Eq. (10):

$$H_{UNB} = \left(1 - \frac{t_u}{t_t}\right) H_t \tag{10}$$

From the mass balance in the column, it is possible to determine the total adsorption capacity q_A (mg g^{-1}), as shown in Eq. (11), as well as the useful adsorption capacity q_b (mg g^{-1}), as exhibited in Eq. (12):

$$q_A = \frac{QC_{A0}}{m_{ads}} \int_0^{t_s} \left(1 - \frac{C_A}{C_{A0}}\right) dt \tag{11}$$

$$q_b = \frac{QC_{A0}}{m_{ads}} \int_0^{t_b} \left(1 - \frac{C_A}{C_{A0}}\right) dt \tag{12}$$

In which, Q is the volumetric flow rate (L min^{-1}) and m_{ads} is the mass of adsorbent to be used in the column. The efficiency of the column can be calculated with the Eq. (13):

$$\mathrm{n} = \frac{q_b}{q_A} \tag{13}$$

To further describe the dynamic adsorption behavior and predict the breakthrough curves, the Bohart–Adams and Yoon–Nelson models were fitted to the experimental data. This model assumes that the rate of adsorption decrease for each adsorbate molecule is proportional to the probability of adsorption and breakthrough. The model is given by Eq. (14):

$$\ln\left(\frac{C_t}{C_0 - C_t}\right) = k_{YN}\,(t - \tau) \tag{14}$$

where C_t is the effluent concentration at time t, k_{YN} (min^{-1}) is the rate constant, and τ is the time required for 50 % breakthrough. The fitting was performed by non-linear regression.

While the Bohart–Adams model (Eq. 15) assumes that the adsorption rate is controlled by surface reactions between the adsorbate and the adsorbent, and that the concentration of the adsorbate in the solid phase is proportional to the residual capacity of the adsorbent [58].

$$\ln\left(\frac{C_t}{C_0}\right) = k_{BA} C_0 t - k_{BA} N_0 \frac{Z}{F} \tag{15}$$

where k_{BA} (L mg^{-1} min^{-1}) is the kinetic constant, N_0 (mg L^{-1}) is the maximum adsorption capacity per unit volume of the adsorbent, Z (cm) is the bed depth and F (cm min^{-1}) is the linear flow velocity.

3. Results and discussion

3.1. Characterization

3.1.1. Textural properties

Table 1 presents the results of the textural properties, which compare the three materials based on surface area. The N_2 adsorption-desorption isotherms at 77 K for all the materials are available in Fig. S1. All materials exhibit noteworthy surface area values; however, AC stands out with significantly higher values than the other materials.

The detailed surface area analysis of AC (S_{BET} = 527 m^2 g^{-1}) indicates the presence of numerous active sites for chemical interactions. The surface area of AC derived from EOP activated with CO_2 can range from 778 to 446 m^2 g^{-1}, as observed by Lustosa et al., who compiled studies on the production of AC from EOP [43]. Also, the average pore width is 1.4 nm, indicating a high micropore presence [43]. In addition, the microporous surface area (S_{mic}) of the AC was found to be 749 m^2 g^{-1}, with a micropore volume (V_{mic}) of 269 mm^3 g^{-1}, further highlighting its significant microporosity and potential for adsorptive applications.

The BET surface area of the CNTs in this study, S_{BET} = 66 m^2 g^{-1}, is somewhat lower than that reported in the review article of Bazargan et al. [59], where CNTs synthesized from LDPE exhibited surface areas around 141 and 74 m^2 g^{-1}. This difference in BET surface area could be attributed to the catalyst composition or to the precursor purity.

Although GP does not surpass the other two materials in this comparison (S_{BET} = 30 m^2 g^{-1}), it remains interesting since its surface area triples compared to its precursor FA (S_{BET} = 13 m^2 g^{-1}). The surface area results for GP are comparable to those observed by Rasaki et al. [60], who, in reviewing several articles, reported that GPs produced from FA have a surface area (S_{BET}) ranging from 10 to 114 m^2 g^{-1}.

The surface area plays a crucial role in adsorption, as it directly correlates with the availability of active sites for the attachment of adsorbates [61]. In this context, materials with higher surface areas, like AC (S_{BET} = 527 m^2 g^{-1}), offer more active sites for chemical interactions; this characteristic enhances adsorption capacity, potentially leading to monolayer adsorption, where adsorbate molecules form a single layer on the surface, or multilayer adsorption, where additional layers accumulate due to intermolecular interactions [62]. Even though GP (S_{BET} = 30 m^2 g^{-1}) have a lower surface area than AC or CNT, they may exhibit other mechanisms, such as ion exchange or surface charge interactions

Table 1
Textural properties analysis of ACs, CNTs and GPs.

Sample	S_{BET} (m^2 g^{-1})	$S_{Langmuir}$ (m^2 g^{-1})	S_{ext} (m^2 g^{-1})	V_{total} (cm^3 g^{-1})
AC	527	782	33	0.3
CNT	66	68	17	0.1
GP	30	42	7	0.07
EOP	14	17	1	0.01
FA	13	15	1	0.01

[63], that enhance their adsorption capacity, particularly for specific adsorbates, like cationic compounds [64].

3.1.2. Surface chemistry

Functional groups in AC, CNT, and GP were analyzed using FT-IR spectroscopy. Fig. 1 presents the results obtained through this method. Comparing the spectra samples reveals differences in the peak intensities and positions [65].

The spectra of AC in Fig. 1a shows the presence of four main peak areas, bands at frequency values were OH stretching in hydroxyl groups in 3431 cm^{-1}, the presence of carbonyl groups (C=O) indicates the presence of oxygen-containing functional groups on the surface of the materials, these groups act as active sites for adsorption and reaction processes, participating in acid-base reactions and hydrogen bonding, as previously assigned in the work [66]. Hydroxyl groups can influence the adsorption behavior of AC by affecting its interaction with water and other molecules; they can increase the affinity of the adsorbent to water, which may impact the adsorption of target contaminants [67]. The C=O stretching vibration at 1636 cm^{-1} indicates chemical stability and bolsters the carbon material's overall robustness and longevity. The C—H deformation vibration at 1383 cm^{-1} reveals the presence of aliphatic hydrocarbons or other organic functional groups on the surface of the adsorbent. These functional groups may facilitate adsorption through interactions with adsorbates mediated by van der Waals or other intermolecular forces [68]. Moreover, the C-O-C vibration at 1022 cm^{-1} attests the incorporation of aromatic rings within the molecular framework [43].

In Fig. 1b is depicted the spectrum of CNTs. This spectrum also displays a hydroxyl group band at 3433 cm^{-1}, as well as a C—O stretching vibration at 1636 cm^{-1} that typically indicates the presence of carbonyl groups and can also reveal the bending vibration of adsorbed water or arising from the absorption of atmospheric CO_2 on the surface of CNTs [69]. In addition, the sharp band at 1390 cm^{-1} confirmed the existence of a C—O bond on raw CNTs, reinforcing the interaction with carboxylate groups [69]. Furthermore, a band at 870 cm^{-1} is attributed to graphitic sp^2 domains [70].

In Fig. 1c is presented the FT-IR spectra for the GP. The characteristic bands of GPs are commonly located at a wavelength range of 1300–900 cm^{-1}. The existing bands in this range are credited to asymmetric stretching vibrations of Al-O-T and Si-O-T, according to He et al. [71]. Also, the Si-O-Si bonds might enhance specific interactions, such as hydrogen bonding or van der Waals forces, thereby improving adsorption efficiency [53]. The narrow band observed at 1637 cm^{-1} is attributed to the bending vibration of H-O-H, indicating the presence of hydroxyl groups from water molecules. A peak around 1014 cm^{-1} followed by a weaker band near 815 cm^{-1} suggests C—O bending vibrations, characteristic of the carbonate ion (CO_3^{2-}) [72]. These bands are likely the result of surface carbonation caused by atmospheric CO_2 interacting with the GP.

The resulting diffraction diagrams are presented in Fig. 2. Several crystalline phases are discernible using the software X′ Pert HighScore Plus in the diffractogram, including calcite, silicate, and aluminum-based phases (Fig. S2).

Calcite, an essential crystalline phase in geopolymeric materials, comprises calcium carbonate ($CaCO_3$) [73]. The presence of silicates is likely attributed to their precursor, sodium silicate (Na_2SiO_3), which may contain some unreacted molecules. In the study by Chao et al. [74], which produced a GP adsorbent using FA from the Manas Power Plant in Xinjiang, China, the XRD analysis results also showed the presence of a quartz phase (a crystalline mineral composed of silica) and a mullite phase (an intermediate phase in the alumina-silica binary system). Finally, the presence of aluminum-based phases is due to the presence of aluminum oxides (Al_2O_3) in the composition of the FA (Table S2), which is also found in studies using FA from MSW in the production of GPs [75].

The pH_{PZC}, acidity, and basicity are crucial parameters for

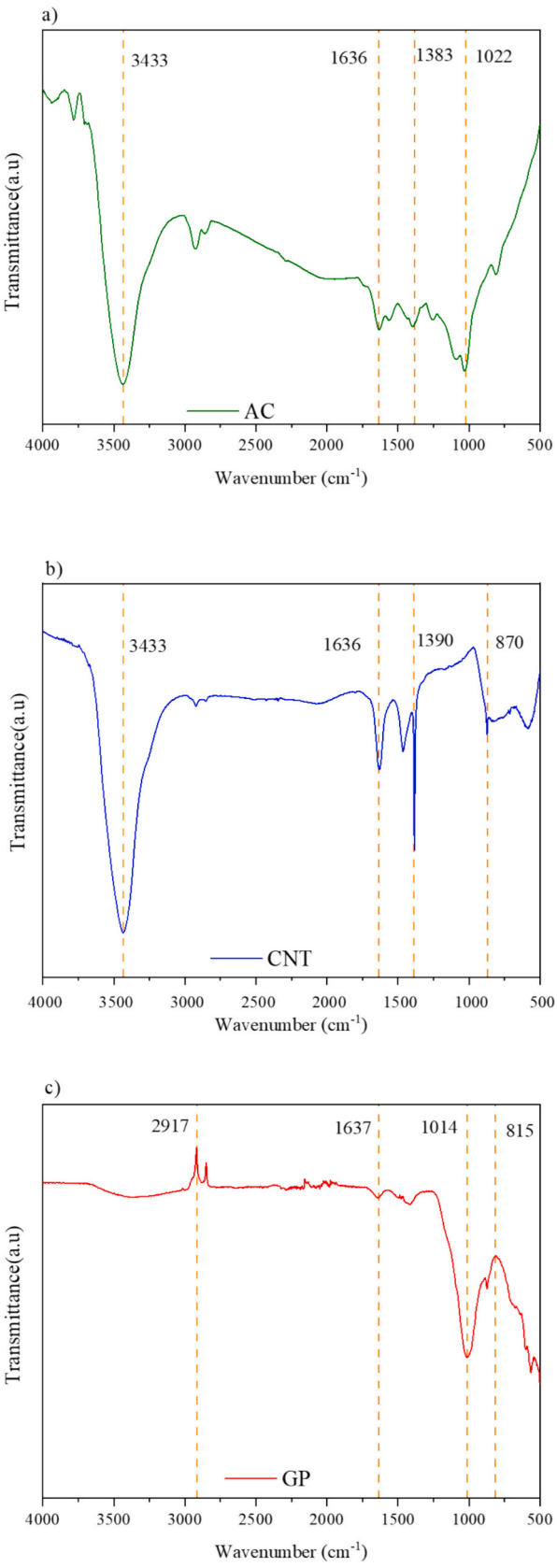

Fig. 1. FT-IR spectra of a) AC, b) CNT, c) GP.

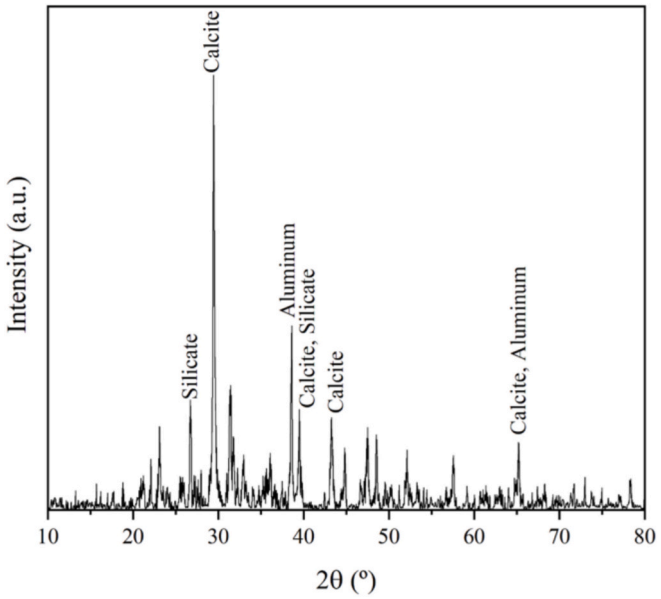

Fig. 2. X-ray diffractogram of geopolymer.

understanding the surface properties of the materials. These parameters dictate how a material interacts with its environment, particularly in adsorption; pH_{PZC} shows that the surface may be positively charged, negatively charged, or have no charge at specific pH values; the acidity and basicity of a material are quantified by the concentration of acidic and basic sites on its surface, usually expressed in micromoles per gram (μmol g^{-1}) [76]. These parameters are shown in Table 2 for each material studied.

AC exhibits a relatively high pH_{PZC} of 9.9. This indicates a predominantly basic surface character. AC has a basicity of 1250 μmol g^{-1} and an acidity of 0 μmol g^{-1}, indicating an entirely basic surface with no detectable acidic sites. This lack of acidic sites and its h high basicity and the pH_{PZC} of 9.9 suggest that AC is particularly effective in adsorbing acidic pollutants and can be used in applications where strong basic interactions are required, such as removing GA [77]. At a pH below 9.9, the surface would attract anions, while above this pH, the surface would be negatively charged and more likely to interact with cations.

CNTs exhibit a pH_{PZC} of 6.9, which is slightly acidic. The study by Abdel-Ghani et al. [69], which used commercial multi-walled CNTs to adsorb phenol and nickel ions, reported a pH_{PZC} of 6.0. This value indicates a surface generally less basic than AC and GP, with a higher tendency to acquire a positive charge at neutral to mildly acidic pH levels. The acidity of CNTs is notably higher, 1360 μmol g^{-1}, while the basicity is lower, 820 μmol g^{-1}, reinforcing the characterization of a surface with a predominantly acidic nature.

The pH_{PZC} of 7.6 for GP indicates a surface near neutral to slightly basic. This value suggests that at pH above 7.6, the GP surface will predominantly carry a negative charge, enhancing its effectiveness in adsorbing cationic species. For instance, in the study by Chao et al. [74], an FA-based GP was used successfully as an adsorbent for Pb^{2+} ions, while Lee et al. [78] made adsorption of Cs^{+}. Conversely, at pH below 7.6, the surface becomes positively charged, favoring the adsorption of anionic species. Ali Siyal et al. [79] demonstrated this effect using an FA-based GP to adsorb anionic surfactants from aqueous solutions. The intermediate pH_{PZC} value of GP reflects its balanced surface chemistry, allowing interaction with a broad range of ionic species. The GP exhibits an acidity of 865 μmol g^{-1} and a basicity of 1925 μmol g^{-1}, with a predominance of basic sites. This balance between acidic and basic functionalities enables the surface of GP to effectively interact with both acidic and basic species, making it versatile for various adsorption applications [80–82].

Table 2
Values of pH_{PZC}, basicity, and acidity.

Sample	pH_{PZC}	Basicity (μmol g^{-1})	Acidity (μmol g^{-1})
AC	9.9	1250	0
CNT	6.9	820	1360
GP	7.6	1925	865

3.1.3. Thermostability

All samples exhibited expected thermal behavior. AC demonstrated moderate thermal stability among the carbon-based materials, while CNT displayed high thermal stability. GP, being inorganic, remained thermally stable even at elevated temperatures. Fig. 3a shows the TGA results and the first-order derivative thermogravimetric analysis (DTG) for AC.

The AC showed an initial mass loss of 13 % compared to its original state due to water evaporation. However, a faster mass loss occurs within 300 to 450 °C temperature range, where the highest DTG peaks are observed. In this range, the oxidation of organic matter begins, but complete combustion only takes place after 500 °C, resulting in a residual mass of 17 % in the form of ash.

Similarly, studies presented by Lustosa et al. [43] on AC from EOP show that, regardless of the activation method, the thermogravimetric behavior experiences a mass reduction at approximately 100 °C (due to water loss), with thermal decomposition starting around 340 °C and stabilizing at 600 °C.

For CNTS, Fig. 3b, DTG analysis shows that the primary mass loss occurs around 650 °C, signifying a strong resistance to oxidation due to the material's robust architecture. This oxidation resistance aligns with the proposed structural models of these nanoscale materials, characterized by dominant aromatic bonds and minimal presence of dangling bonds. The CNTs experience oxidation at this point, leading to a substantial mass decrease. Complete combustion is achieved only beyond 700 °C, leaving behind 7.9 % residual ash, which can be attributed to metals coming from residual CVD catalyst [44].

The TGA and DTG for the GP, the only inorganic material, are present in Fig. 3c. The DTG analysis reveals a significant mass loss at around 100 °C, attributed to water evaporation, which is expected and consistent with the findings in the literature [83,84]. The rapid decrease in mass before 150 °C is indicative of the evaporation of both chemically bound water within the GP structure and free water. Following this, there is a gradual but minor mass loss due to the elimination of hydroxyl groups (-OH) and chemically bonded water.

However, around 655 °C, another peak in mass loss is observed. According to He et al. [83], this second weight loss, typically occurring between 300 and 650 °C, is related to the dehydroxylation of Si-OH, Al-OH, and Ca-OH groups. The final stage of mass loss, often appearing above 750 °C and associated with the decomposition of carbonate species, was not observed in this GP. Ultimately, the residual mass stands at 86 %, which is close to the 79 % found in fly ash-based GPs in the study by Abdulkareem et al. [84].

3.2. Contaminant adsorption

3.2.1. Kinetic modeling

This study conducted nine kinetic experiments, following the logic presented in Table 3. For each contaminant, the three different materials were tested to evaluate the rate and efficiency of the adsorption process. The kinetic models represented by eqs. 3–5 were fitted to experimental data of the adsorption kinetics.

The kinetic tests were performed using pollutant solutions without any pH adjustment. After mixing the adsorbent with the adsorbate, the pH values of the solutions were measured. AC, with a high pH_{PZC} of 9.9 and a basicity of 1250 μmol g^{-1}, exhibited a pH values close to the neutral (7.0 for ACT, 7.4 for SMX, and 7.8 for GA) when in contact with

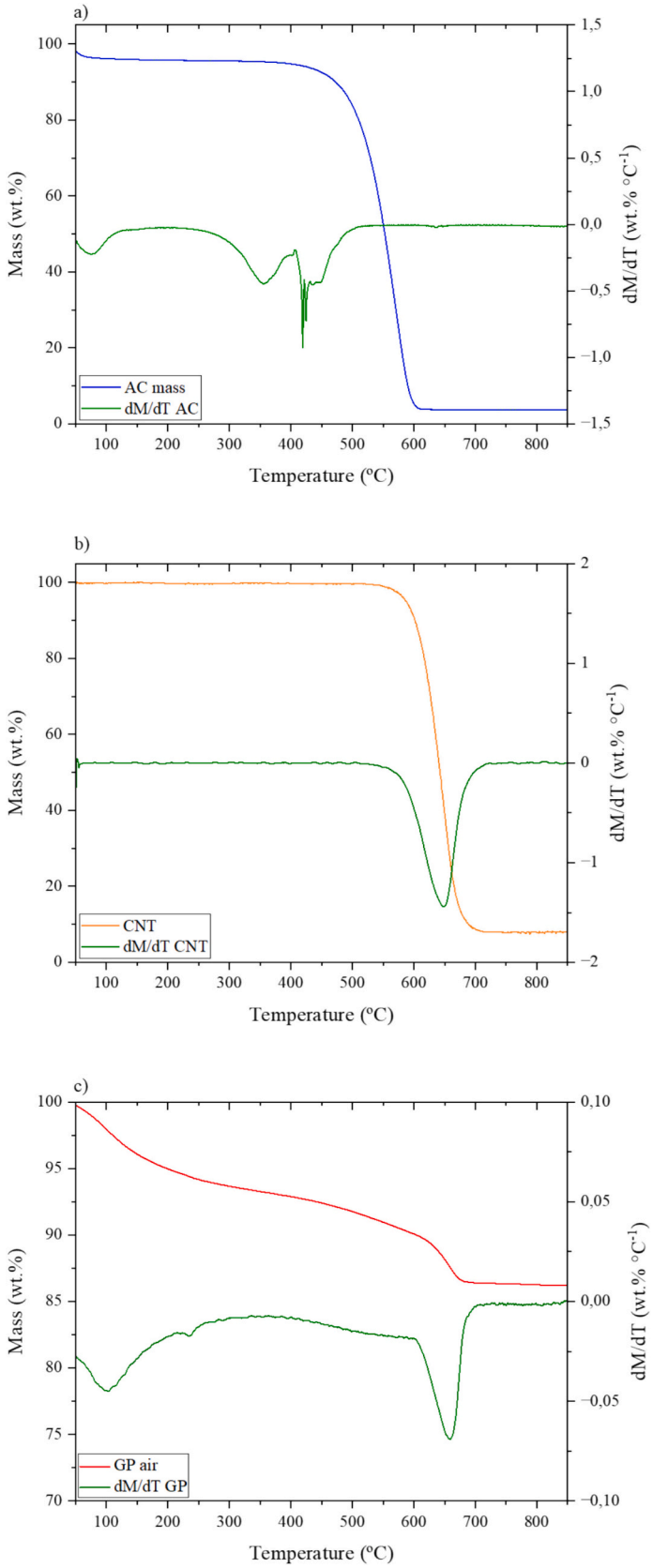

Fig. 3. Thermogravimetric analysis in air (TGA and DTG) for: a) AC; b) CNT; and c) GP.

Table 3
Parameters of adsorption kinetic models for pseudo-first and second order and intraparticle diffusion.

Pollutant	Sample	Pseudo-first order				Pseudo-second order			Intraparticle diffusion		
		q_{exp} (mg g^{-1})	q_e (mg g^{-1})	K_1 (min^{-1})	r^2	q_e (mg g^{-1})	K_2 (g mg^{-1} min^{-1})	r^2	I (mg g^{-1})	K_{id} (mg g^{-1} $min^{-0.5}$)	r^2
ACT	AC	40.4	37.7	0.23	0.96	39.7	0.00	0.99	20.0	1.49	0.53
	CNT	12.0	9.3	0.35	0.82	9.8	0.05	0.88	5.1	0.38	0.55
	GP	0.6	0.5	0.13	0.94	0.6	0.32	0.97	0.2	0.02	0.60
SMX	AC	36.2	29.5	0.03	0.83	33.3	0.00	0.91	6.2	1.65	0.82
	CNT	25.5	24.5	0.37	0.94	25.4	0.02	0.92	16.6	0.66	0.28
	GP	4.0	4.9	1.38	0.48	4.8	0.00	0.48	3.3	0.15	0.23
GA	AC	35.8	34.8	0.55	0.97	36.0	0.02	0.99	24.4	0.96	0.29
	CNT	28.6	25.6	0.50	0.86	27.0	0.02	0.99	16.2	0.95	0.47
	GP	17.5	17.4	0.25	0.99	18.3	0.02	0.97	10.8	0.56	0.34

the pollutants. This suggests that AC maintains a relatively neutral environment for adsorption, likely due to its lack of surface acidity. In contrast, CNT, with a lower pH_{PZC} of 6.9, showed more acidic pH values (4.8 for ACT, 4.5 for SMX, and 3.8 for GA), which is consistent with its higher acidity (1360 μmol g^{-1}). The lower pH_{PZC} of CNT indicates that the adsorbent surface tends to be negatively charged at neutral pH, leading to stronger interactions with acidic pollutants and a tendency to acidify the solution. GP, with an intermediate pH_{PZC} of 7.6, showed relatively stable pH values (6.6 for ACT, 6.9 for SMX, and 7.6 for GA), reflecting its more neutral surface charge and a balanced combination of acidity (865 μmol g^{-1}) and basicity (1925 μmol g^{-1}). This suggests that GP has a more balanced surface interaction with the pollutants, leading to less pronounced pH changes.

Analysis of Table 3 reveals notable findings, including the absence of intraparticle diffusion effects, indicating limited internal transport within particles, and the dominance of the pseudo-second-order model, suggesting chemisorption as the primary adsorption mechanism. As described by Wang et al. [85], internal diffusion models assume that the diffusion of the adsorbate within the adsorbent is the rate-limiting step. In this context, the diffusion of the adsorbate in the liquid film surrounding the adsorbent and the adsorption onto active sites are not instantaneous [86]. Furthermore, while the pseudo-first order and pseudo-second order models yielded high r^2 values in the fitting process, the pseudo-second-order model provided the best fit, suggesting an abundance of active sites on the adsorbent.

The results obtained for adsorption capacities of ACT and GA correlate with S_{BET} of the materials (0.97 for S_{BET} *vs* $q_{e,ACT}$ and 0.81 for pH_{PZC} *vs* $q_{e,GA}$), whereas SMX adsorption has a weaker correlation with S_{BET} (0.57 for S_{BET} *vs* $q_{e,SMX}$), as shown in Figs. S3a, S3c, and S3e. The total pore volume (V_T) also correlates strongly with the adsorption capacities obtained in the pseudo-second-order model (0.99 for V_T *vs.* $q_{e,ACT}$, 0.63 for V_T *vs.* $q_{e,SMX}$, and 0.85 for V_T *vs.* $q_{e,GA}$), as shown in Figs. S3b, S3d, and S3f. The weaker correlation between textural properties and SMX adsorption suggests that surface chemistry plays a more significant role in the adsorption of this compound compared to ACT and GA. No correlation was found between adsorption capacities and acid/basic characterizations (*i.e.*, pH_{PZC}, acidity, and basicity).

Considering the parameter q_e and comparing it with the q_{exp}, the values are closely aligned, thereby validating its applicability in describing the adsorption kinetics data. Moreover, when assessing the adsorption capacity of the materials across the three different contaminants, AC performed the best in pseudo-second order and achieved values of 39.7 mg g^{-1}, 33.3 mg g^{-1}, and 36.0 mg g^{-1} for ACT, SMX, and GA, respectively. Consequently, adsorption equilibrium is reached more quickly for AC and GA in the pseudo-first-order model, with K_1 of 0.55, and for GP with ACT in the pseudo-second-order model, with a K_2 of 0.32. In the study by Pérez et al. [67], the adsorption kinetics of GA with different ACs were analyzed. Regardless of the precursor material or production method, the kinetics fit the pseudo-second-order equation. Further, Fig. 4 presents the experimental points for each kinetic study across the different adsorbent/adsorbate groups and the previous optimal fittings.

AC demonstrated the best results for all three pollutants. For instance, AC reached 64 % of its adsorption capacity within 5 min for ACT, a value comparable to that found in the work of Nguyen et al. [87]; In this study, a commercial AC oxidized with HNO_3 increased oxygen-functional groups (S_{BET} = 1284 m^2 g^{-1}), removing approximately 52 % of ACT from the solution within the first 5 min of contact. The best fit for this study was achieved using the pseudo-second-order model.

For SMX, AC also exhibited good adsorption capacity (33.3 mg g^{-1}) and performance, demonstrating its efficiency as an adsorbent. Other studies applying commercial ACs for SMX removal from water also achieved good results. This was observed both at low concentrations (2 μg L^{-1} and 2 mg L^{-1} of SMX with 10 mg L^{-1} of AC), as naturally found in tap water, as reported by Gutiérres et al. [88], where their commercial powdered AC achieved effective removal, and at higher concentrations (an adsorbent dosage of 0.05 g L^{-1} and a series of initial SMX concentrations 20–100 mg L^{-1}), as demonstrated by Yawei Shi et al. [89].

Finally, when analyzing the performance of AC for GA removal, which was also satisfactory (36 mg g^{-1}), and comparing it with the review work by Ho et al. [90], the removal of GA using different ACs ranges from 1.7 to 48.3 mg g^{-1}. According to Lustosa et al. [25], microporous ACs from EOPs offer enhanced adsorption capacity due to their high surface area and strong van der Waals forces within the confined pores, confirming the results obtained in the characterization of the material's surface area (S_{BET} = 527 m^2 g^{-1}), acidity (0 μmol g^{-1}), and basicity (1250 μmol g^{-1}).

CNTs demonstrated to be an intermediate material, showing adsorption capacities of 9.8 mg g^{-1} for ACT, 25.4 mg g^{-1} for SMX, and 27.0 mg g^{-1} for GA. In literature, CNTs are primarily applied as catalysts in advanced oxidation processes. Still, some papers focused on modifying the surface chemistry of CNTs to improve their adsorption efficiency. For instance, Kusmierek et al. [91]. reported adsorption capacities of 28.8, 17.9, and 38.8 mg g^{-1} for ACT, using regular CNTs and CNTs functionalized with hydroxyl and carboxyl groups, respectively. The result obtained by the author using CNTs is higher due to the higher surface areas of the CNTs used in their work (S_{BET} = 154–179 m^2 g^{-1}). Ameen et al. [92]. reported 58.5 mg g^{-1} adsorption capacity of SMX in multi-walled CNTs, demonstrating that pH also influences the process (more efficient at acidic pH). The higher adsorption capacity reported in their work is also related to the higher surface area in that case (S_{BET} = 500 m^2 g^{-1}). For instance, Tuesta et al. [44] tested CNTs synthesized from LDPE *via* CVD in catalytic wet peroxide oxidation and found that these CNTs could adsorb 11 % (4.4 mg g^{-1}) to 31 % (12.4 mg g^{-1}) of ACT at an initial concentration of 100 μg mL^{-1}.

The GP showed an affinity for adsorbing GA (q_e = 18.3 mg g^{-1}). Hijazi et al. [93] demonstrated that GPs derived from FA and modified with titanium oxide can reach a q_e = 166.7 mg g^{-1}. In a comprehensive review of GP application for heavy metal and dye removal, Liang K. *et al* [94] summarized several studies focused on removing cationic dyes, which are particularly effective due to their negative surface charge and the alkaline conditions created by the activators. For instance, Acisli

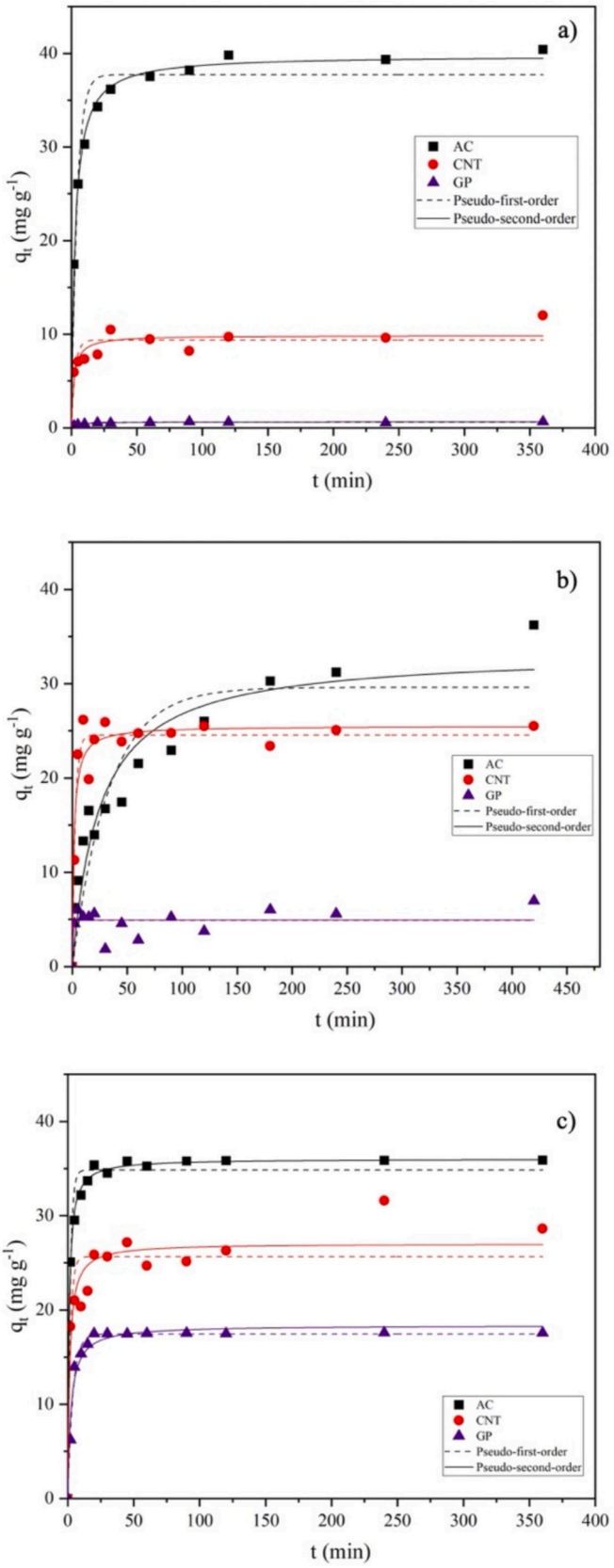

Fig. 4. Fitting the adsorption kinetic models to the experimental data obtained for a) ACT; b) SMX; and c) GA pollutants with each adsorbent (AC - activated carbon, CNT - carbon nanotube and GP - Geopolymer, C_{ads} = 2.5 g L^{-1}, $C_{ACT,\ SMX\ and\ GA}$ = 100 mg L^{-1}, agitation = 300 rpm).

et al. [64] efficiently removed Basic Yellow 2, while Zhang et al. [95] and Wattanasiriwech et al. [96] successfully removed Methylene Blue using FA-based geopolymers and foam mortar, respectively. These materials demonstrate strong electrostatic interactions that facilitate cationic dye adsorption, as the negatively charged geopolymer surfaces attract the positively charged dye molecules, enhancing the adsorption process. Our material also exhibited adsorption through electrostatic interactions, which is characteristic of cationic GP. The pH_{PZC} of the GP was 7.6, indicating that the surface charge of the materials is negative at neutral and basic pH. Additionally, the measured basicity (1925 μmol g^{-1}) and acidity value of (865 μmol g^{-1}) further emphasize the alkaline nature of the material.

It is also noticeable that the rate at which all three materials reach equilibrium is quite similar; in the initial minutes, all materials can achieve maximum adsorption.

3.2.2. *Equilibrium isotherms*

The equilibrium isotherms were studied by fitting Langmuir and Freundlich's models described by eqs. 6 and 7, respectively, to AC, CNT, and GP. Table 4 presents the parameters obtained from the equilibrium fits.

By analyzing the r^2 values for the systems, it is evident that the Freundlich model provides a better fit for the compounds ACT (0.96 for AC, 0.93 for CNT, and 0.90 for GP), SMX (0.99 for AC and 0.93 for GP), and GA (0.99 for AC, and 0.97 for CNT) while Langmuir fitted better specifically for SMX with CNT (0.93) and GA with GP (0.93). The adsorbent/adsorbate interactions likely follow the description of Freundlich adsorption on a non-uniform (heterogeneous) surface, with interactions between adsorbed molecules in a reversible and non-ideal adsorption process rather than adsorption on a monolayer surface. All the values of $1/n_f$ were <1, indicating that the adsorption is favorable, and that the adsorbate is preferentially adsorbed at higher concentrations.

The results from the Langmuir model show that AC exhibited excellent adsorption performance, with maximum adsorption capacities of 112.1 mg g^{-1}, 40.2 mg g^{-1}, and 314.2 mg g^{-1} for ACT, SMX, and GA, respectively, highlighting its affinity and effectiveness as an adsorbent across different compounds. In contrast, CNT and GP exhibited moderate adsorption capacities for ACT, with values of 18.4 mg g^{-1} for CNT and 11.6 mg g^{-1} for GP. Similarly, for SMX, CNTs reached a q_{max} of 14.7 mg g^{-1}, while GP reached 5.6 mg g^{-1}. However, for GA, both CNTs and GPs demonstrated satisfactory performance, with q_{max} values of 66.1 mg g^{-1} and 97.8 mg g^{-1}, respectively. When compared to other adsorbents reported in the literature, such as diatomite used by Song et al. [34] for GA removal (q_{max} = 19.5 mg·g^{-1}) or magnetic chitosan reported by Chai et al. [97] (q_{max} = 48.39 mg g^{-1}), it is evident that CNTs and GPs offer competitive and promising adsorption capacities, particularly for GA.

The Langmuir isotherm parameter (K_L) was used to calculate R_L, indicating the solute's affinity presented in Table 5. When R_L = 0, the

Table 4
Equilibrium model parameters determined in the adsorption of ACT, SMX and GA for AC, CNT and GP adsorbents.

Pollutant	Sample	Langmuir			Freundlich		
		q_{max} (mg g^{-1})	K_L (L mg^{-1})	r^2	K_F (L g^{-1})	n_F	r^2
ACT	AC	112.1	5.14	0.90	62.9	4.65	0.96
	CNT	18.4	0.01	0.85	0.97	2.14	0.93
	GP	11.6	0.50	0.90	0.47	1.15	0.90
SMX	AC	40.2	0.24	0.92	148	4.32	0.99
	CNT	14.7	0.01	0.93	0.90	2.21	0.88
	GP	5.6	0.01	0.93	0.02	1.12	0.93
GA	AC	314.2	0.03	0.99	12.6	1.36	0.99
	CNT	66.1	0.02	0.83	8.5	2.78	0.97
	GP	97.8	0.18	0.96	24.2	3.46	0.87

Table 5
R_L calculated values for AC.

C_0 (mg L^{-1})	AC			CNT			GP		
	ACT	SMX	GA	ACT	SMX	GA	ACT	SMX	GA
100	0.002	0.039	0.248	0.555	0.558	0.641	0.022	0.506	0.060
75	0.003	0.052	0.305	0.632	0.632	0.757	0.029	0.580	0.077
50	0.004	0.075	0.397	0.729	0.735	0.929	0.044	0.671	0.114
30	0.006	0.120	0.523	0.869	0.961	0.984	0.086	0.962	0.209
10	0.019	0.290	0.767	0.934	0.963	0.992	0.333	0.961	0.581

adsorption process is considered irreversible. If $0 < R_L < 1$, the process is considered favorable to adsorption. A value of $R_L = 1$ signifies a linear process, while $R_L > 1$ indicates an unfavorable adsorption process [53].

All calculated values fall between 0 and 1, indicating that the adsorption process is favorable. However, the values for adsorption of ACT using AC were notably low, which may suggest an irreversible process at higher concentrations [53].

Fig. 5 presents the isotherm plots showing the fit of the two equilibrium models (Langmuir and Freundlich) for the best-performing adsorbent (AC). The corresponding isotherms for the other materials (GP and CNT) are provided in Fig. S4. These graphs visually illustrate how well the models align with the experimental data.

It is interesting to relate the shape of the graphs in Fig. 5: AC (C_{ads} = 2.5 g L^{-1}) adsorption isotherms using Langmuir and Freundlich for a) ACT; b) SMX; and c) GA which shows that adsorption is strongly favorable for ACT (q_{max} = 112.1 mg g^{-1}) and SMX (q_{max} = 40.2 mg g^{-1}) and for GA (q_{max} = 314.2 mg g^{-1}). These results can be attributed to the fundamental properties of AC, as shown in its acidity and basicity tests. Since the contaminants are primarily acidic, they are likely to exhibit higher adsorption capacities due to this pH compatibility. Furthermore, the high surface area of AC (S_{BET} = 527 m^2 g^{-1}) enhances its adsorption capacity, enabling effective pollutant removal. In a study on the removal of CECs using different materials, Alsalihy et al. [17] highlighted that ACs are highly effective in removing this class of pollutants, achieving adsorption capacities of 320 mg g^{-1} for diclofenac and 280 mg g^{-1} for naproxen. Consequently, due to their simplicity, lower cost, and high effectiveness, ACs may offer significant advantages over conventional methods such as ozonation, UV disinfection, and activated sludge processes [98].

3.2.3. Breakthrough curves and Yoon-Nelson modeling: single and multiple compounds

Table 6 presents the breakthrough curve parameters and Yoon–Nelson model fitting results for each compound (ACT, SMX and GA). The analysis was first conducted with individual compounds and subsequently with a simulated solution containing all three pollutants. The fixed-bed column was packed with 20 g of GP and 0.5 g of AC powder. This combination was selected to exploit the synergistic effect between GP and AC, with GP serving as a structural support to minimize AC dispersion while also participating in the adsorption process.

The breakthrough curve in single compounds mode demonstrates that the system required 314 min to reach breakthrough for ACT, 66 min for SMX, and 68 min for GA. These results were obtained using concentrations of 100 mg L^{-1} for each compound, a flow rate of 1 mL min^{-1}, and room temperature. The breakthrough time was determined when the effluent concentration reached 5 % of the initial concentration. Moreover, the compounds' useful adsorption capacity (q_b) in continuous mode showed that ACT achieved a value of 62.8 mg g^{-1}, while the other two compounds reached values around 13 mg g^{-1}. These capacities were calculated based on the bed's usable capacity time. Still, if the bed is used until complete stoichiometric exhaustion, the values increase to 126.9 mg g^{-1}, 54.9 mg g^{-1}, and 151.6 mg g^{-1} for ACT, SMX, and GA, respectively.

The mass-transfer zone is represented by H_{UNB}. Small values of this parameter mean that the breakthrough curve is close to an ideal step with negligible mass-transfer resistance. Moreover, in the ideal condition, no axial dispersion would occur [57]. Fig. 6a shows the breakthrough curve for each contaminant in a separate system.

In breakthrough curves, the areas above the curve correspond to the adsorption capacity, while the areas below the curve refer to the concentration in the effluent stream [99]. It is important to note that these experiments lasted for 1440 min. The column efficiency is also calculated based on the valuable and total adsorption capacity. As a result, systems that reached 5 % of the effluent concentration earlier exhibited lower efficiency, even though total breakthroughs did not occur as quickly as in the case of GA. On the other hand, the system for ACT and SMX removal showed an efficiency of 49.5 % and 24.1 %, respectively.

To further evaluate the dynamic behavior of the adsorption process, the Yoon-Nelson model was applied to the breakthrough data in single compound (Fig. 6a). The high coefficients of determination (r^2 = 0.96 for ACT and for SMX, and 0,93 for GA) confirm the model's suitability in describing the breakthrough behavior. The kinetic constant (k) remained low (0.01–0.02 min^{-1}), indicating a relatively slow rate of adsorption consistent with the observed breakthrough delays. Notably, the characteristic time required for 50 % breakthrough (τ) closely followed the breakthrough order observed experimentally, 475 min for ACT, 156 min for SMX, and 328 min for GA, reinforcing the higher affinity and capacity of the bed for ACT.

The behavior of the multiple compounds followed a similar to that observed in the single system; however, it is evident that the column reached saturation much earlier, as the active sites of the adsorbent materials were consumed more rapidly. This can be observed in Table 6, which presents the parameters from the analysis of this breakthrough curve. The molar fractions of each compound are identical. Comparing the values of the bed's usable capacity with the tests conducted for each compound individually, the multicomponent system's time was reduced by an average of 26 %. As expected, the adsorption capacity was also altered in the same proportion. This aligns with the findings of Chang et al. [100], who observed a granular AC in the competitive adsorption of three pharmaceuticals (ACT, diclofenac, and SMX). According to their study, the competitive interactions are influenced predominantly by macropore characteristics, with mesopores and micropores playing a secondary role. These competitive effects are particularly relevant for real-world systems, where multiple compounds coexist in complex matrices and can interfere with one another's adsorption.

The application of the Yoon-Nelson model to the multicomponent system (Fig. 6b) further corroborates the competitive effects. While the model maintained good correlation (r^2 = 0.98 for ACT, 0,96 for SMX, and 0,94 for GA), a decrease in τ values was observed, 341 min for ACT, 151 min for SMX, and 314 min for GA, compared to the single-compound scenario. This decline quantitatively reflects the earlier saturation of the adsorbent bed, attributed to site competition.

Although the Yoon-Nelson model was successfully applied in this study, the Bohart–Adams model is also frequently used to describe breakthrough behavior, especially in the initial adsorption phase [58]. It considers parameters like bed depth and influent concentration, making it useful for scale-up. However, due to its simplifying assumptions, the neglect of axial dispersion and film diffusion resistance, the Bohart–Adams model did not yield satisfactory fits in this case. The coefficient of determination values were below acceptable thresholds for

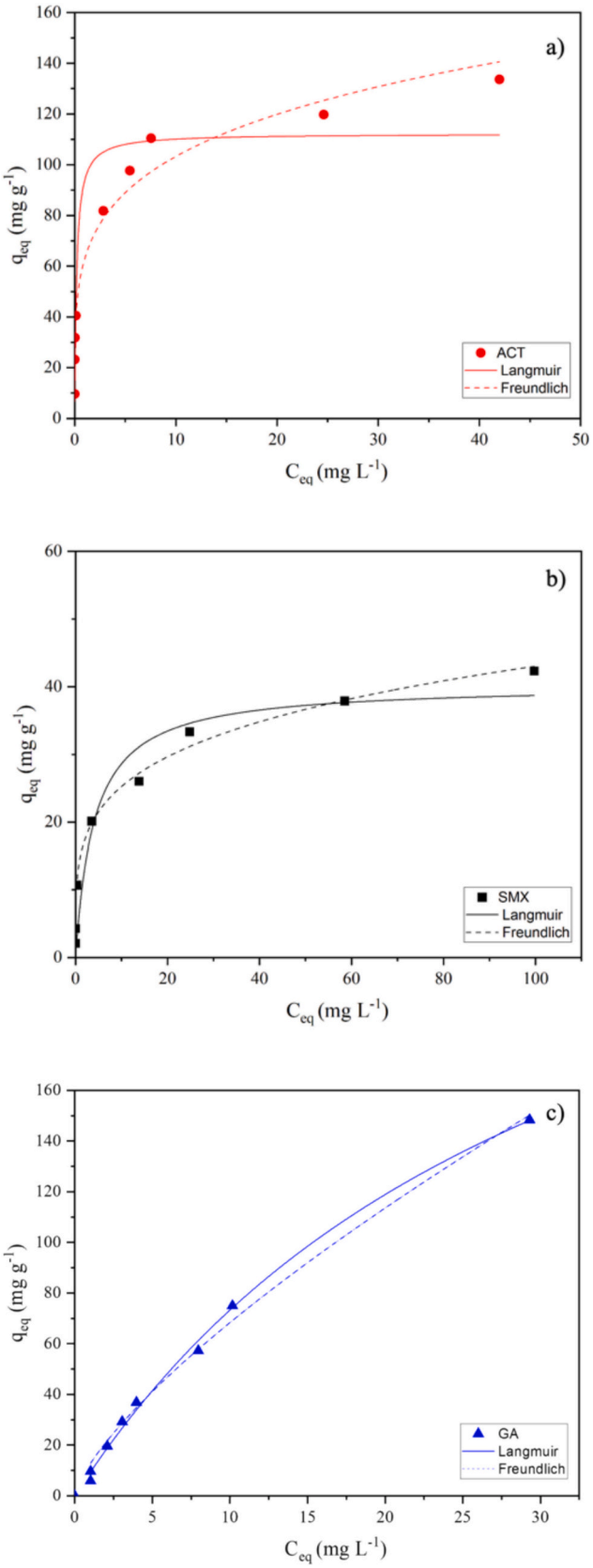

Fig. 5. AC (C_{ads} = 2.5 g L^{-1}) adsorption isotherms using Langmuir and Freundlich for a) ACT; b) SMX; and c) GA ($C_{ACT,\ SMX\ and\ GA}$ = 15, 25, 50, 75, 100, 150, 200, and 400 mg L^{-1}).

both single and multicomponent systems, indicating poor predictive capability. In single-component systems, r^2 values were 0.35 for SMX, 0.39 for GA, and 0.53 for ACT. In multicomponent systems, the values were 0.26 for SMX, 0.41 for GA, and 0.54 for ACT.

4. Conclusions

Eco-friendly adsorbents were synthesized, from real solid wastes and used to remove pollutants like acetaminophen, sulfamethoxazole, and a phenolic compound (gallic acid) from wastewater. The study underscores the advantages of adopting a circular economy approach by converting waste materials into high-value adsorbents, addressing waste management challenges and environmental remediation needs. Among the tested materials, activated carbon exhibited the highest adsorption capacity, achieving maximum values of 112.2 mg g^{-1} for ACT, 40.3 mg g^{-1} for SMX, and 314.3 mg g^{-1} for GA, with Freundlich isotherms providing the best fit for the adsorption process. This superior performance can be attributed to AC's high surface area (527 m^2 g^{-1}) which favor interactions with acidic pollutants like GA. The kinetic modeling further confirmed the pseudo-second-order model as the best fit, indicating that chemisorption mechanisms primarily governed the adsorption process.

The breakthrough curve analysis in continuous flow shows that AC an exhibited significant breakthrough times (314 min for ACT, 66 min for SMX, and 68 min for GA) in single-component systems. In multicomponent systems, competitive adsorption effects reduced the time to breakthrough, as expected, but the material's overall adsorption efficiency remained robust. The GPs and CNTs also displayed promising adsorption properties, particularly in specific applications. GPs were more suited for cationic pollutant removal due to their balanced acidic and basic surface properties (pH_{PZC} = 7.6). Finally, combining these materials in composite systems could present synergistic effects, offering tailored solutions for complex wastewater matrices.

For future research, regeneration and reuse of the adsorbents will be a key focus, especially considering the practical implementation of these materials. Given the variety of materials studied, different regeneration methodologies will be evaluated. Additionally, the application of combined treatment processes, such as coagulation, advanced oxidation processes or biological treatments with adsorption, is a promising avenue to enhance the treatment of real pharmaceutical wastewater.

CRediT authorship contribution statement

Ana Paula Ferreira: Writing – review & editing, Writing – original draft, Visualization, Methodology, Investigation, Formal analysis, Data curation, Conceptualization. **Arthur P. Baldo:** Writing – original draft, Methodology, Investigation, Formal analysis. **Adriano S. Silva:** Writing – review & editing, Investigation. **Ana Paula S. Natal:** Investigation. **Ana J.B. Bezerra:** Investigation. **Jose L. Diaz de Tuesta:** Writing – review & editing, Visualization, Supervision, Funding acquisition, Conceptualization. **Pricila Marin:** Supervision. **José A. Peres:** Writing – review & editing, Visualization, Supervision, Funding acquisition. **Helder T. Gomes:** Writing – review & editing, Visualization, Supervision, Project administration, Funding acquisition, Conceptualization.

Declaration of Generative AI and AI-assisted technologies in the writing process

While preparing this work, the authors used ChatGPT to reduce the manuscript size and improve readability. After using this tool, the authors reviewed and edited the content as needed and took full responsibility for the publication's content.

Declaration of competing interest

The authors declare that they have no known competing financial

Table 6
Breakthrough curve and Yoon–Nelson fitting parameters for individual and mixed pollutants.

Compound		t_u (min)	t_t (min)	q_A (mg g^{-1})	q_b (mg g^{-1})	H_U (cm)	H_{UNB} (cm)	n (%)	Yoon-Nelson r^2	Yoon-Nelson k (min)	Yoon-Nelson τ (min)
Single compound adsorption runs	ACT	314.2	634.2	126.8	62.8	1.5	1.5	49.5	0.96	0.01	475
	SMX	66.1	274.6	54.9	13.2	0.7	2.3	24.0	0.96	0.02	156
	GA	68.2	758.1	151.6	13.6	0.2	2.8	9.0	0.93	0.00	314
Multiple compounds adsorption run	ACT	228.6	444.3	88.8	45.7	1.5	1.5	51.4	0.98	0.01	341
	SMX	46.0	227.4	45.4	9.2	0.6	2.4	20.2	0.96	0.02	151
	GA	53.5	521.6	104.3	10.7	0.3	2.7	10.2	0.94	0.00	286

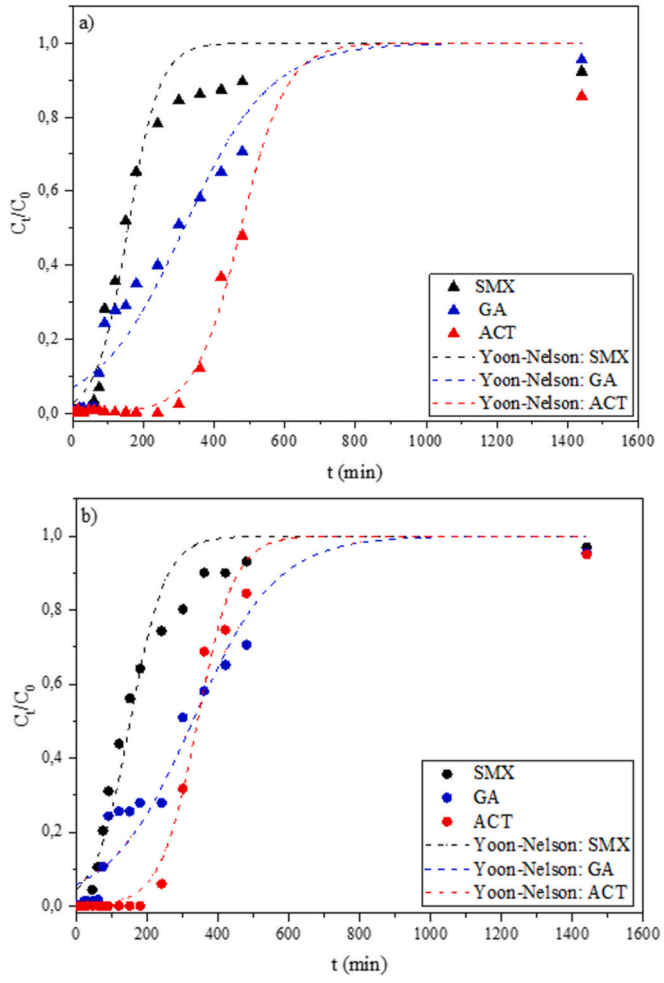

Fig. 6. Breakthrough curves of adsorption and Yoon-Nelson model fit: a) isolated pollutants system and b) multi-components system. (GP = 20 g, AC = 0.5 g, $C_{ACT,\ SMX\ and\ GA}$ = 100 mg L^{-1} - either mixed or separated, Q = 0.1 mL min^{-1}).

interests or personal relationships that could have appeared to influence the work reported in this paper.

Acknowledgments

This work was supported by national funds supported this work through FCT/MCTES (PIDDAC): CIMO, UIDB/00690/2020 (DOI: 10.54499/UIDB/00690/2020) and UIDP/00690/2020 (DOI: 10.54499/UIDP/00690/2020); and SusTEC, LA/P/0007/2020 (DOI: 10.54499/LA/P/0007/2020). We would also like to thank the scientific collaboration under Base-UIDB/50020/2020, CQVR (UIDB/00616/2020). The authors are grateful to Sociedade Ponto Verde for the financial support through the project "Avaliação de Ciclo de Vida de materiais geopoliméricos obtidos a partir da valorização de resíduos sólidos urbanos". Ana Paula Silva is supported by the doctoral grant PRT/BD/153090/2021 financed by FCT and with funds from NORTE2020, under MIT Portugal Program. Jose L. Diaz De Tuesta acknowledges the financial support through the program of *Atracción al Talento* of *Comunidad de Madrid* (Spain) for the individual research grant and project with reference 2022-T1/AMB-23946; and through the program *Consolidación Investigadora 2024* (CNS2024-154264) supported from *Agencia Estatal de Investigación* (Spain).

Appendix A. Supplementary data

Supplementary data to this article can be found online at https://doi.org/10.1016/j.jwpe.2025.107914.

Data availability

All information is available in the article and supplementary material.

References

[1] J.C.G. Sousa, A.R. Ribeiro, M.O. Barbosa, M.F.R. Pereira, A.M.T. Silva, A review on environmental monitoring of water organic pollutants identified by EU guidelines, J. Hazard. Mater. 344 (2018) 146–162, https://doi.org/10.1016/j.jhazmat.2017.09.058.
[2] E.J. Tiedeken, A. Tahar, B. McHugh, N.J. Rowan, Monitoring, sources, receptors, and control measures for three European Union watch list substances of emerging concern in receiving waters – a 20 year systematic review, Sci. Total Environ. 574 (2017) 1140–1163, https://doi.org/10.1016/j.scitotenv.2016.09.084.
[3] W.F. DIRECTIVE, Common implementation strategy for the water framework directive (2000/60/EC), Guidance Document (2003) 7.
[4] E.U.W. Directive, Council Directive of 21. May 1991 Concerning urban waste water treatment (91/271/EEC), J. Eur. Commun. (1991) 34–40.
[5] B.A. Mohamed, H. Hamid, C.V. Montoya-Bautista, L.Y. Li, Circular economy in wastewater treatment plants: treatment of contaminants of emerging concerns (CECs) in effluent using sludge-based activated carbon, J. Clean. Prod. 389 (2023) 136095, https://doi.org/10.1016/j.jclepro.2023.136095.
[6] O. Golovko, S. Örn, M. Sörengård, K. Frieberg, W. Nassazzi, F.Y. Lai, L. Ahrens, Occurrence and removal of chemicals of emerging concern in wastewater treatment plants and their impact on receiving water systems, Sci. Total Environ. 754 (2021) 142122, https://doi.org/10.1016/j.scitotenv.2020.142122.
[7] R.K. Mishra, S.S. Mentha, Y. Misra, N. Dwivedi, Emerging pollutants of severe environmental concern in water and wastewater: a comprehensive review on current developments and future research, Water-Energy Nexus 6 (2023) 74–95, https://doi.org/10.1016/j.wen.2023.08.002.
[8] J.L. Martinez, Environmental pollution by antibiotics and by antibiotic resistance determinants, Environ. Pollut. 157 (2009) 2893–2902, https://doi.org/10.1016/j.envpol.2009.05.051.
[9] S. Wacławek, K. Krawczyk, D. Silvestri, V.V.T. Padil, M. Řezanka, M. Černík, M. Jaroniec, Cyclodextrin-based strategies for removal of persistent organic pollutants, Adv. Colloid Interf. Sci. 310 (2022) 102807, https://doi.org/10.1016/j.cis.2022.102807.
[10] M. Li, S. Huang, X. Yu, W. Zhao, S. Lyu, Q. Sui, Discharge of pharmaceuticals from a municipal solid waste transfer station: overlooked influence on the contamination of pharmaceuticals in surface waters, Sci. Total Environ. 839 (2022) 156317, https://doi.org/10.1016/j.scitotenv.2022.156317.
[11] A.K. Priya, S. Antony, G.M.S. Kumar, S. Sivamoorthi, S. Vineesh, Anthropogenic impacts on the contamination in the coastal region: a review, Mater Today Proc 37 (2021) 2236–2238, https://doi.org/10.1016/j.matpr.2020.07.681.
[12] T. Rasheed, M. Bilal, F. Nabeel, M. Adeel, H.M.N. Iqbal, Environmentally-related contaminants of high concern: potential sources and analytical modalities for

detection, quantification, and treatment, Environ. Int. 122 (2019) 52–66, https://doi.org/10.1016/j.envint.2018.11.038.
[13] W. Feng, Y. Deng, F. Yang, Q. Miao, S.K. Ngien, Systematic review of contaminants of emerging concern (CECs): distribution, risks, and implications for water quality and health, Water (Basel) 15 (2023) 3922, https://doi.org/10.3390/w15223922.
[14] J.C. Espíndola, N. Scaccia, I. Barbosa Segundo, D. da S. Diniz, J.U. Diniz, J. C. Mierzwa, Evaluation of the pathway of contaminants in the environment: a case study of different aquatic environmental compartments, Sustainability 16 (10) (2024) 3927, https://doi.org/10.3390/su16103927.
[15] J. Wilkinson, P.S. Hooda, J. Barker, S. Barton, J. Swinden, Occurrence, fate and transformation of emerging contaminants in water: an overarching review of the field, Environ. Pollut. 231 (2017) 954–970, https://doi.org/10.1016/j.envpol.2017.08.032.
[16] A. Ayaliew Werkneh, S. Berhe Gebru, G.H. Redae, A. Gashaw Tsige, Removal of endocrine disrupters from the contaminated environment: public health concerns, treatment strategies and future perspectives-a review, Heliyon 8 (2022), https://doi.org/10.1016/j.heliyon.2022.e09206, 1–12.
[17] S.T.H. Alsalihy, A.N. Ahmed, G.H.A. Salih, M.J. M-Ridha, O.A. AL Falahi, Removal of pharmaceutical and personal care products (PhPCPs) using different low-cost materials as substrates in the vertical, horizontal, and hybrid flow systems of constructed wetlands – a review, Environ. Technol. Innov. 35 (2024) 103647, https://doi.org/10.1016/j.eti.2024.103647.
[18] G. Singh, A. Singh, V. Kumar Mishra, A critical review of occurrence, sources, fate, ecological risk, and health effect of emerging contaminants in water and wastewater, Environ Nanotechnol Monit Manag 22 (2024) 100994, https://doi.org/10.1016/j.enmm.2024.100994.
[19] A.S. Silva, P.Z. Filho, A.P. Ferreira, F.F. Roman, A.P. Baldo, M. Rauhauser, J. L. Diaz de Tuesta, A.I. Pereira, A.M.T. Silva, J.M.T. Pietrobelli, M. S. Kalmakhanova, D.D. Snow, H.T. Gomes, Occurrence of micropollutants in surface water and removal by catalytic wet peroxide oxidation enhanced filtration using polymeric membranes loaded with carbon nanotubes, Chemical Engineering Journal Advances 21 (2025) 100707, https://doi.org/10.1016/j.ceja.2025.100707.
[20] R.E. Campbell, C.H. Chen, C.L. Edelstein, Overview of antibiotic-induced nephrotoxicity, Kidney Int Rep 8 (2023) 2211–2225, https://doi.org/10.1016/j.ekir.2023.08.031.
[21] S. Chen, Z. Shen, J. Ding, M. Qu, T. Li, M. Tong, Y. Di, Sulfamethoxazole induced systematic and tissue-specific antioxidant defense in marine mussels (Mytilus galloprovincialis): implication of antibiotic's ecotoxicity, Chemosphere 279 (2021) 130634, https://doi.org/10.1016/j.chemosphere.2021.130634.
[22] B. Zhang, Y. He, W. Shi, L. Liu, L. Li, C. Liu, P.N.L. Lens, Biotransformation of sulfamethoxazole (SMX) by aerobic granular sludge: removal performance, degradation mechanism and microbial response, Sci. Total Environ. 858 (2023) 159771, https://doi.org/10.1016/j.scitotenv.2022.159771.
[23] G.I. Scott, D.E. Porter, R.S. Norman, C.H. Scott, M.I. Uyaguari-Diaz, K.A. Maruya, S.B. Weisberg, M.H. Fulton, E.F. Wirth, J. Moore, P.L. Pennington, D. Schlenk, G. P. Cobb, N.D. Denslow, Antibiotics as CECs: an overview of the hazards posed by antibiotics and antibiotic resistance, Front. Mar. Sci. 3 (2016), https://doi.org/10.3389/fmars.2016.00024.
[24] L.H.M.L.M. Santos, M. Gros, S. Rodriguez-Mozaz, C. Delerue-Matos, A. Pena, D. Barceló, M.C.B.S.M. Montenegro, Contribution of hospital effluents to the load of pharmaceuticals in urban wastewaters: identification of ecologically relevant pharmaceuticals, Sci. Total Environ. 461–462 (2013) 302–316, https://doi.org/10.1016/j.scitotenv.2013.04.077.
[25] X. Qu, M. Tian, B. Liao, A. Chen, Enhanced electrochemical treatment of phenolic pollutants by an effective adsorption and release process, Electrochim. Acta 55 (2010) 5367–5374, https://doi.org/10.1016/j.electacta.2010.04.089.
[26] N. Solomakou, A.M. Goula, Treatment of olive mill wastewater by adsorption of phenolic compounds, Rev. Environ. Sci. Biotechnol. 20 (2021) 839–863, https://doi.org/10.1007/s11157-021-09585-x.
[27] A. Arditsoglou, D. Voutsa, Partitioning of endocrine disrupting compounds in inland waters and wastewaters discharged into the coastal area of Thessaloniki, northern Greece, Environ. Sci. Pollut. Res. 17 (2010) 529–538, https://doi.org/10.1007/s11356-009-0172-y.
[28] M. Zhou, J. Zhang, C. Sun, Occurrence, ecological and human health risks, and seasonal variations of phenolic compounds in surface water and sediment of a potential polluted river basin in China, Int. J. Environ. Res. Public Health 14 (2017) 1140, https://doi.org/10.3390/ijerph14101140.
[29] C. Mateescu, E.-M. Lungulescu, N.-O. Nicula, Effectiveness of biological approaches for removing persistent organic pollutants from wastewater: a mini-review, Microorganisms 12 (2024) 1632, https://doi.org/10.3390/microorganisms12081632.
[30] U. Hübner, S. Spahr, H. Lutze, A. Wieland, S. Rüting, W. Gernjak, J. Wenk, Advanced oxidation processes for water and wastewater treatment – guidance for systematic future research, Heliyon 10 (2024) e30402, https://doi.org/10.1016/j.heliyon.2024.e30402.
[31] Z. Al-Qodah, T.M. Al-Zghoul, A. Jamrah, The performance of pharmaceutical wastewater treatment system of electrocoagulation assisted adsorption using perforated electrodes to reduce passivation, Environ. Sci. Pollut. Res. 31 (2024) 20434–20448, https://doi.org/10.1007/s11356-024-32458-z.
[32] M.S. Akhtar, S. Ali, W. Zaman, Innovative adsorbents for pollutant removal: exploring the latest research and applications, Molecules 29 (2024) 4317, https://doi.org/10.3390/molecules29184317.
[33] Z. Kang, X. Jia, Y. Zhang, X. Kang, M. Ge, D. Liu, C. Wang, Z. He, A review on application of biochar in the removal of pharmaceutical pollutants through adsorption and persulfate-based AOPs, Sustainability 14 (2022) 10128, https://doi.org/10.3390/su141610128.
[34] X. Song, C. Li, Z. Chai, Y. Zhu, Y. Yang, M. Chen, R. Ma, X. Liang, J. Wu, Application of diatomite for gallic acid removal from molasses wastewater, Sci. Total Environ. 765 (2021) 142711, https://doi.org/10.1016/j.scitotenv.2020.142711.
[35] Y. Luo, G. Huang, Y. Li, Y. Yao, J. Huang, P. Zhang, S. Ren, J. Shen, Z. Zhang, Removal of pharmaceutical and personal care products (PPCPs) by MOF-derived carbons: a review, Sci. Total Environ. 857 (2023) 159279, https://doi.org/10.1016/j.scitotenv.2022.159279.
[36] S. Wong, N. Ngadi, I.M. Inuwa, O. Hassan, Recent advances in applications of activated carbon from biowaste for wastewater treatment: a short review, J. Clean. Prod. 175 (2018) 361–375, https://doi.org/10.1016/j.jclepro.2017.12.059.
[37] H. Jin, Y. Zhang, Q. Wang, Q. Chang, C. Li, Rapid removal of methylene blue and nickel ions and adsorption/desorption mechanism based on geopolymer adsorbent, Colloid Interface Sci Commun 45 (2021) 100551, https://doi.org/10.1016/j.colcom.2021.100551.
[38] N. Mu'azu, N. Jarrah, M. Zubair, O. Alagha, Removal of phenolic compounds from water using sewage sludge-based activated carbon adsorption: a review, Int. J. Environ. Res. Public Health 14 (2017) 1094, https://doi.org/10.3390/ijerph14101094.
[39] A. Santos Silva, F.F. Roman, A.P.F. da Silva, J.L. Diaz de Tuesta, M. Kalmakhanova, D. Snow, H.T. Gomes, Reactive Materials and Solutions Towards Treatment and Reuse of Waters with Contaminants of Emerging Concern, 2024, pp. 477–488, https://doi.org/10.1007/978-3-031-48532-9_44.
[40] W.J. Lee, P.S. Goh, W.J. Lau, A.F. Ismail, Removal of pharmaceutical contaminants from aqueous medium: a state-of-the-art review based on paracetamol, Arab. J. Sci. Eng. 45 (2020) 7109–7135, https://doi.org/10.1007/s13369-020-04446-1.
[41] İ. Kara, D. Yilmazer, S.T. Akar, Metakaolin based geopolymer as an effective adsorbent for adsorption of zinc(II) and nickel(II) ions from aqueous solutions, Appl. Clay Sci. 139 (2017) 54–63, https://doi.org/10.1016/j.clay.2017.01.008.
[42] X. Ma, M. Tsige, S. Uddin, S. Talapatra, Application of carbon nanotubes for removing organic contaminants from water, Mater. Express 1 (2011) 183–200, https://doi.org/10.1166/mex.2011.1023.
[43] J.F. Lustosa Filho, A.P.F. da Silva, S.T. Costa, H.T. Gomes, T. de Figueiredo, Z. Hernández, Biochars derived from olive mill byproducts: typology, characterization, and eco-efficient application in agriculture—a systematic review, Sustainability 16 (2024) 5004, https://doi.org/10.3390/su16125004.
[44] J.L. Diaz de Tuesta, A.S. Silva, F.F. Roman, L.F. Sanches, F.A. da Silva, A. I. Pereira, A.M.T. Silva, J.L. Faria, H.T. Gomes, Polyolefin-derived carbon nanotubes as magnetic catalysts for wet peroxide oxidation of paracetamol in aqueous solutions, Catal. Today 419 (2023) 114162, https://doi.org/10.1016/j.cattod.2023.114162.
[45] N.B. Singh, B. Middendorf, Geopolymers as an alternative to Portland cement: an overview, Constr. Build. Mater. 237 (2020) 117455, https://doi.org/10.1016/j.conbuildmat.2019.117455.
[46] J. Majtacz, H.E. Al-Hazmi, X. Xu, G. Piechota, X. Li, G. Kumar, T.M. Aminabhavi, M.R. Saeb, M. Badawi, J. Mąkinia, Removal of nitrogen from wastewater: unsolved problems and possible solutions with partial denitrification/anammox systems, Chem. Eng. J. 499 (2024) 156131, https://doi.org/10.1016/j.cej.2024.156131.
[47] A. Gizaw, F. Zewge, A. Kumar, A. Mekonnen, M. Tesfaye, A comprehensive review on nitrate and phosphate removal and recovery from aqueous solutions by adsorption, J. Water Supply Res. Technol. AQUA 70 (2021) 921–947, https://doi.org/10.2166/aqua.2021.146.
[48] H. Chen, Y.J. Zhang, P.Y. He, C.J. Li, L.C. Liu, Novel activated carbon route to low-cost geopolymer based porous composite with high mechanical resistance and enhanced CO2 capacity, Microporous Mesoporous Mater. 305 (2020) 110282, https://doi.org/10.1016/j.micromeso.2020.110282.
[49] I. Luhar, S. Luhar, M.M.A.B. Abdullah, R.A. Razak, P. Vizureanu, A.V. Sandu, P.-D. Matasaru, A state-of-the-art review on innovative geopolymer composites designed for water and wastewater treatment, Materials 14 (2021) 7456, https://doi.org/10.3390/ma14237456.
[50] P. Chang, S. Zhou, T. Wang, D. Hua, S. Liu, O.V. Okoro, A. Shavandi, L. Nie, Eco-friendly carbon nanotubes reinforced with sodium alginate/polyacrylic acid for enhanced adsorption of copper ions: kinetics, isotherm, and mechanism adsorption studies, Molecules 29 (2024) 4518, https://doi.org/10.3390/molecules29194518.
[51] D.A. Khuong, H.N. Nguyen, T. Tsubota, Activated carbon produced from bamboo and solid residue by CO2 activation utilized as CO2 adsorbents, Biomass Bioenergy 148 (2021) 106039, https://doi.org/10.1016/j.biombioe.2021.106039.
[52] F.F. Roman, A.S. Silva, J.L. Diaz de Tuesta, A.P. Baldo, J.P.M. Lopes, G. Gonçalves, A.I. Pereira, P. Praça, A.M.T. Silva, J.L. Faria, M. Bañobre-López, H. T. Gomes, Plastic waste-derived carbon nanotubes: influence of growth catalyst and catalytic activity in CWPO, J. Environ. Chem. Eng. 13 (2025) 115206, https://doi.org/10.1016/j.jece.2024.115206.
[53] A.P. Ferreira, A.P.S. Natal, A.P. Baldo, A.S. Silva, J.L. Diaz de Tuesta, P. Marin, J. A. Peres, H.T. Gomes, Response surface method-driven design of experiments for the synthesis of fly ash-based geopolymers in the gallic acid optimized removal from wastewater, Chemical Engineering Journal Advances 21 (2025) 100703, https://doi.org/10.1016/j.ceja.2024.100703.
[54] E.F.L. Moraes, A.P.F. da Silva, J.L. Diaz de Tuesta, A.N. Silva, F. Orssatto, H. T. Gomes, Production of polymeric membranes based on activated carbons for

wastewater treatment, in: The 4th International Electronic Conference on Applied Sciences, MDPI, Basel Switzerland, 2023, p. 336, https://doi.org/10.3390/ASEC2023-16874.
[55] L. Li, S. Wang, Z. Zhu, Geopolymeric adsorbents from fly ash for dye removal from aqueous solution, J. Colloid Interface Sci. 300 (2006) 52–59, https://doi.org/10.1016/J.JCIS.2006.03.062.
[56] A.A. Abin-Bazaine, M.A. Olmos-Marquez, A. Campos-Trujillo, A fixed-bed column sorption: breakthrough curves modeling, in: Sorption - New Perspectives and Applications [Working title], IntechOpen, 2024, https://doi.org/10.5772/intechopen.1004446.
[57] T.O. Chaplina, Y.D. Chashechkin, E.V. Stepanova, Flows induced by sorption on fibrous material in a two-layer oil−water system, Dokl. Phys. 61 (2016) 444–448, https://doi.org/10.1134/S1028335816090019.
[58] Z. Al-Qodah, M. Al-Shannag, B. Hudaib, W. Bani-Salameh, A.T. Shawaqfeh, E. Assirey, Synergy and enhanced performance of combined continuous treatment processes of pre-chemical coagulation (CC), solar-powered electrocoagulation (SAEC), and post-adsorption for dairy wastewater, Case Studies in Chemical and Environmental Engineering 11 (2025) 101183, https://doi.org/10.1016/j.cscee.2025.101183.
[59] A. Bazargan, G. McKay, A review – synthesis of carbon nanotubes from plastic wastes, Chem. Eng. J. 195 (2012) 377–391, https://doi.org/10.1016/j.cej.2012.03.077.
[60] S.A. Rasaki, Z. Bingxue, R. Guarecuco, T. Thomas, Y. Minghui, Geopolymer for use in heavy metals adsorption, and advanced oxidative processes: a critical review, J. Clean. Prod. 213 (2019) 42–58, https://doi.org/10.1016/j.jclepro.2018.12.145.
[61] P.V. Mane, R.M. Rego, P.L. Yap, D. Losic, M.D. Kurkuri, Unveiling cutting-edge advances in high surface area porous materials for the efficient removal of toxic metal ions from water, Prog. Mater. Sci. 146 (2024) 101314, https://doi.org/10.1016/j.pmatsci.2024.101314.
[62] X. Liu, Q. Hao, M. Fan, B. Teng, Carbonaceous adsorbents in wastewater treatment: from mechanism to emerging application, Sci. Total Environ. 955 (2024) 177106, https://doi.org/10.1016/j.scitotenv.2024.177106.
[63] A.M. Elgarahy, A. Maged, M.G. Eloffy, M. Zahran, S. Kharbish, K.Z. Elwakeel, A. Bhatnagar, Geopolymers as sustainable eco-friendly materials: classification, synthesis routes, and applications in wastewater treatment, Sep. Purif. Technol. 324 (2023) 124631, https://doi.org/10.1016/j.seppur.2023.124631.
[64] O. Acisli, I. Acar, A. Khataee, Preparation of a fly ash-based geopolymer for removal of a cationic dye: isothermal, kinetic and thermodynamic studies, J. Ind. Eng. Chem. 83 (2020) 53–63, https://doi.org/10.1016/j.jiec.2019.11.012.
[65] X. Feng, S. Yan, S. Jiang, K. Huang, X. Ren, X. Du, P. Xing, Green synthesis of the metakaolin/slag based geopolymer for the effective removal of methylene blue and Pb(II), Silicon 14 (2022) 6965–6979, https://doi.org/10.1007/S12633-021-01439-Z. /METRICS.
[66] R. Labied, O. Benturki, A.Y. Eddine Hamitouche, A. Donnot, Adsorption of hexavalent chromium by activated carbon obtained from a waste lignocellulosic material (*Ziziphus jujuba* cores): kinetic, equilibrium, and thermodynamic study, Adsorpt. Sci. Technol. 36 (2018) 1066–1099, https://doi.org/10.1177/0263617417750739. /ASSET/IMAGES/LARGE/10.1177_0263617417750739-FIG 13.JPEG.
[67] B. Petrovic, M. Gorbounov, S. Masoudi Soltani, Impact of surface functional groups and their introduction methods on the mechanisms of CO_2 adsorption on porous carbonaceous adsorbents, Carbon Capture Sci. Technol. 3 (2022) 100045, https://doi.org/10.1016/J.CCST.2022.100045.
[68] I.K. Tetteh, I. Issahaku, A.Y. Tetteh, Recent advances in synthesis, characterization, and environmental applications of activated carbons and other carbon derivatives, Carbon Trends 14 (2024) 100328, https://doi.org/10.1016/j.cartre.2024.100328.
[69] N.T. Abdel-Ghani, G.A. El-Chaghaby, F.S. Helal, Individual and competitive adsorption of phenol and nickel onto multiwalled carbon nanotubes, J. Adv. Res. 6 (2015) 405–415, https://doi.org/10.1016/J.JARE.2014.06.001.
[70] T. Maiyalagan, B. Viswanathan, Template synthesis and characterization of well-aligned nitrogen containing carbon nanotubes, Mater. Chem. Phys. 93 (2005) 291–295, https://doi.org/10.1016/J.MATCHEMPHYS.2005.03.039.
[71] P. He, K. Xin, X. Zhang, Z. Guo, W. Zheng, Development of an activated carbon-geopolymer composite for treatment of Pb(II) polluted water and soil, Int. J. Appl. Ceram. Technol. 20 (2023) 3027–3040, https://doi.org/10.1111/ijac.14393.
[72] L. Panda, S.S. Rath, D.S. Rao, B.B. Nayak, B. Das, P.K. Misra, Thorough understanding of the kinetics and mechanism of heavy metal adsorption onto a pyrophyllite mine waste based geopolymer, J. Mol. Liq. 263 (2018) 428–441, https://doi.org/10.1016/j.molliq.2018.05.016.
[73] S. Tome, A. Nana, H.K. Tchakouté, J. Temuujin, C.H. Rüscher, Mineralogical evolution of raw materials transformed to geopolymer materials: a review, Ceram. Int. 50 (2024) 35855–35868, https://doi.org/10.1016/j.ceramint.2024.07.024.
[74] Y. Chao, M. Zhao, X. Ma, D. Chen, H. Guo, Y. Liao, Novel organic–inorganic geopolymer composite materials for removing Pb2+ from wastewater, Mater. Lett. 330 (2023), https://doi.org/10.1016/j.matlet.2022.133401.
[75] N. Ariffin, M.M.A.B. Abdullah, P. Postawa, S. Zamree Abd Rahim, M.R.R. Mohd Arif Zainol, R. Putra Jaya, A. Śliwa, M.F. Omar, J.J. Wysłocki, K. Błoch, M. Nabiałek, Effect of aluminium powder on kaolin-based geopolymer characteristic and removal of Cu^{2+}, Mater 14 (2021) 814, https://doi.org/10.3390/ma14040814.
[76] M. Kosmulski, The pH dependent surface charging and points of zero charge. X. Update, Adv. Colloid Interf. Sci. 319 (2023) 102973, https://doi.org/10.1016/j.cis.2023.102973.
[77] A. Chedri Mammar, L. Mouni, J.-C. Bollinger, L. Belkhiri, A. Bouzaza, A.A. Assadi, H. Belkacemi, Modeling and optimization of process parameters in elucidating the adsorption mechanism of Gallic acid on activated carbon prepared from date stones, Sep. Sci. Technol. 55 (2020) 3113–3125, https://doi.org/10.1080/01496395.2019.1676785.
[78] N.K. Lee, H.R. Khalid, H.K. Lee, Adsorption characteristics of cesium onto mesoporous geopolymers containing nano-crystalline zeolites, Microporous Mesoporous Mater. 24 (2017) 238–244, https://doi.org/10.1016/J.MICROMESO.2017.01.030.
[79] A.A. Siyal, M.R. Shamsuddin, N.E. Rabat, M. Zulfiqar, Z. Man, A. Low, Fly ash based geopolymer for the adsorption of anionic surfactant from aqueous solution, J. Clean. Prod. 229 (2019) 232–243, https://doi.org/10.1016/J.JCLEPRO.2019.04.384.
[80] D. Dong, K. Wang, M. Yi, Y. Liang, Y. Muhammad, E. Wei, Y. Wei, T. Fujita, Preparation of TiO2 photocatalyst microspheres by geopolymer technology for the degradation of tetracycline, J. Clean. Prod. 339 (2022), https://doi.org/10.1016/j.jclepro.2022.130734.
[81] J. Qiu, Y. Zhao, J. Xing, X. Sun, Fly ash-based geopolymer as a potential adsorbent for Cr(VI) removal, Desalination Water Treat 70 (2017) 201–209, https://doi.org/10.5004/DWT.2017.20493.
[82] E. Sitarz-Palczak, J. Kalembkiewicz, Application of halloysite geopolymers to removal of methyl blue from aqueous solution, International Journal of GEOMATE 21 (2021) 87–94, https://doi.org/10.21660/2021.87.j2330.
[83] R. He, N. Dai, Z. Wang, Thermal and mechanical properties of Geopolymers exposed to high temperature: a literature review, Advances in Civil Engineering 2020 (2020) 7532703, https://doi.org/10.1155/2020/7532703.
[84] O.A. Abdulkareem, A.M. Mustafa Al Bakri, H. Kamarudin, I. Khairul Nizar, A. A. Saif, Effects of elevated temperatures on the thermal behavior and mechanical performance of fly ash geopolymer paste, mortar, and lightweight concrete, Constr. Build. Mater. 50 (2014) 377–387, https://doi.org/10.1016/J.CONBUILDMAT.2013.09.047.
[85] J. Wang, X. Guo, Adsorption kinetic models: physical meanings, applications, and solving methods, J. Hazard. Mater. 390 (2020), https://doi.org/10.1016/J.JHAZMAT.2020.122156.
[86] A. Samadi, L. Kong, W. Guo, M. Sillanpää, I. Boztepe, C. Song, Q. Zeng, S. Zhao, Standardized methodology for performance evaluation in using polyaniline-based adsorbents to remove aqueous contaminants, J. Environ. Chem. Eng. 12 (2024) 112650, https://doi.org/10.1016/j.jece.2024.112650.
[87] D.T. Nguyen, H.N. Tran, R.S. Juang, N.D. Dat, F. Tomul, A. Ivanets, S.H. Woo, A. Hosseini-Bandegharaei, V.P. Nguyen, H.P. Chao, Adsorption process and mechanism of acetaminophen onto commercial activated carbon, J. Environ. Chem. Eng. 8 (2020) 104408, https://doi.org/10.1016/J.JECE.2020.104408.
[88] M. Gutiérrez, P. Verlicchi, D. Mutavdžić Pavlović, Study of the influence of the wastewater matrix in the adsorption of three pharmaceuticals by powdered activated carbon, Molecules 28 (2023) 2098, 28 (2023) 2098, https://doi.org/10.3390/MOLECULES28052098.
[89] Y. Shi, G. Liu, L. Wang, H. Zhang, Activated carbons derived from hydrothermal impregnation of sucrose with phosphoric acid: remarkable adsorbents for sulfamethoxazole removal, RSC Adv. 9 (2019) 17841–17851, https://doi.org/10.1039/C9RA02610J.
[90] S. Ho, Low-cost adsorbents for the removal of phenol/phenolics, pesticides, and dyes from wastewater systems: a review, Water (Basel) 14 (2022) 3203, https://doi.org/10.3390/w14203203.
[91] K. Kuśmierek, L. Dąbek, A. Świątkowski, The use of modified multi-walled carbon nanotubes for the removal of selected pharmaceuticals from the aqueous environment, Desalination Water Treat 288 (2023) 60–71, https://doi.org/10.5004/dwt.2023.29140.
[92] H. Mohamed Ameen, S. Kunsági-Máté, P. Noveczky, L. Szente, B. Lemli, Adsorption of sulfamethazine drug onto the modified derivatives of carbon nanotubes at different pH, Molecules 25 (2020) 2489, https://doi.org/10.3390/molecules25112489.
[93] D.A. Hijazi, A. BiBi, M.A. Al-Ghouti, Sustainable waste utilization: geopolymeric fly ash waste as an effective phenol adsorbent for environmental remediation, Resources, Environment and Sustainability 15 (2024) 100142, https://doi.org/10.1016/j.resenv.2023.100142.
[94] K. Liang, X.Q. Wang, C.L. Chow, D. Lau, A review of geopolymer and its adsorption capacity with molecular insights: a promising adsorbent of heavy metal ions, J. Environ. Manag. 322 (2022) 116066, https://doi.org/10.1016/j.jenvman.2022.116066.
[95] X. Zhang, X. Zhou, T.B. Moghaddam, F. Zhang, F. Otto, Synergistic effects of iron (Fe) and biochar on light-weight geopolymers when used in wastewater treatment applications, J. Clean. Prod. 322 (2021) 129033, https://doi.org/10.1016/j.jclepro.2021.129033.
[96] D. Wattanasiriwech, K. Yomthong, S. Wattanasiriwech, Adsorption efficiency and photocatalytic activity of fly ash-based geopolymer foam mortar, Ceram. Int. 47 (2021) 27361–27371, https://doi.org/10.1016/j.ceramint.2021.06.158.
[97] Z. Chai, C. Li, Y. Zhu, X. Song, M. Chen, Y. Yang, D. Chen, X. Liang, J. Wu, Arginine-modified magnetic chitosan: preparation, characterization and adsorption of gallic acid in sugar solution, Int. J. Biol. Macromol. 165 (2020) 506–516, https://doi.org/10.1016/j.ijbiomac.2020.09.141.
[98] L. Rizzo, S. Malato, D. Antakyali, V.G. Beretsou, M.B. Đolić, W. Gernjak, E. Heath, I. Ivancev-Tumbas, P. Karaolia, A.R. Lado Ribeiro, G. Mascolo, C.S. McArdell, H. Schaar, A.M.T. Silva, D. Fatta-Kassinos, Consolidated vs new advanced treatment methods for the removal of contaminants of emerging concern from

urban wastewater, Sci. Total Environ. 655 (2019) 986–1008, https://doi.org/10.1016/j.scitotenv.2018.11.265.

[99] A. Gómez-Avilés, M. Peñas-Garzón, C. Belver, J.J. Rodriguez, J. Bedia, Equilibrium, kinetics and breakthrough curves of acetaminophen adsorption onto activated carbons from microwave-assisted FeCl3-activation of lignin, Sep. Purif. Technol. 278 (2021) 119654, https://doi.org/10.1016/j.seppur.2021.119654.

[100] E.E. Chang, J.C. Wan, H. Kim, C.H. Liang, Y.D. Dai, P.C. Chiang, Adsorption of selected pharmaceutical compounds onto activated carbon in dilute aqueous solutions exemplified by acetaminophen, diclofenac, and sulfamethoxazole, Sci. World J. 2015 (2015), https://doi.org/10.1155/2015/186501.